Chinese Society of Aeronautics and Astronautics
& Beihang University

**Chinese Journal of Aeronautics**

cja@buaa.edu.cn
www.sciencedirect.com

# Decentralized adaptive sliding mode control of a space robot actuated by control moment gyroscopes

CrossMark

**Jia Yinghong** \*, Xu Shijie

School of Astronautics, Beihang University, Beijing 100083, China

**Abstract**   An adaptive sliding mode control (ASMC) law is proposed in decentralized scheme for trajectory tracking control of a new concept space robot. Each joint of the system is a free ball joint capable of rotating with three degrees of freedom (DOF). A cluster of control moment gyroscopes (CMGs) is mounted on each link and the base to actuate the system. The modified Rodrigues parameters (MRPs) are employed to describe the angular displacements, and the equations of motion are derived using Kane's equations. The controller for each link or the base is designed separately in decentralized scheme. The unknown disturbances, inertia parameter uncertainties and nonlinear uncertainties are classified as a "lumped" matched uncertainty with unknown upper bound, and a continuous sliding mode control (SMC) law is proposed, in which the control gain is tuned by the improved adaptation laws for the upper bound on norm of the uncertainty. A general amplification function is designed and incorporated in the adaptation laws to reduce the control error without conspicuously increasing the magnitude of the control input. Uniformly ultimate boundedness of the closed loop system is proved by Lyapunov's method. Simulation results based on a three-link system verify the effectiveness of the proposed controller.

© 2016 Chinese Society of Aeronautics and Astronautics. Production and hosting by Elsevier Ltd. This is an open access article under the CC BY-NC-ND license (http://creativecommons.org/licenses/by-nc-nd/4.0/).

## 1. Introduction

Space robot has been playing an important role in space service missions. Accurate trajectory tracking control is commonly required to complete the operations such as refuelling and module replacing. However, the nonlinear dynamical coupling between the base motion and manipulator arm motion makes the control very complex and incapacitates the direct application of the control algorithms for terrestrial robotic systems to space systems. To achieve superior system performance of a space robot, extensive researches focusing on control algorithms have been carried out, which are subject to different missions and problems.[1–6]

However, in general, system performance depends upon not only the active control schemes and algorithms, but also the dynamical characteristics. Traditional space robots are actuated by joint torque actuators. When the joint torque is exerted on the manipulator arm, the reaction torque is also exerted on

\* Corresponding author. Tel.: +86 10 82339750.
  E-mail address: jia_yingh@163.com (Y. Jia).
Peer review under responsibility of Editorial Committee of CJA.

the base. Such action/reaction torques definitely increase the dynamical coupling between the base and arm, and hence decrease system performance. To eliminate or reduce the dynamical coupling, the concept of "reactionless actuator" was proposed for space robots or robot-like space multibody systems. Billing-Ross and Wilson designed a reactionless drive pointing system, and summarized several advantages of reactionless actuation over traditional actuation.[7]

One typical concept of reactionless space robot is actuating the system using angular momentum exchange devices instead of joint torque actuators. In the design concept, the manipulator links are connected via free rotational joints, and the links are driven by angular momentum exchange devices, such as control moment gyroscopes (CMGs) or reaction wheels, mounted on the links. Since the actuating torques are directly exerted on the moving bodies (links or the base) and the joints are free, the action/reaction torques about the joints do not exist anymore, and consequently the dynamical coupling could be expected to be eliminated or reduced. In 1994, Osuka et al.[8] proposed a design concept of space manipulator called "torque-unit manipulator". In the design concept, each joint is free joint with one degree of freedom (DOF), and a DC-servo motor is mounted on each link to accelerate or decelerate a wheel hence to actuate the link motion. Though the concept was proposed mainly for easy maintenance, it is indeed a reactionless space robot design. Later, Peck et al.[9,10] applied CMGs to rigid robotic systems, and compared power consumption of the systems employing CMGs actuation, reaction wheel actuation and joint torque actuation. They pointed out that the CMGs actuating manipulator arm reduces the reaction torque on the base in comparison with joint actuating arm, and the system with CMGs actuation can radically outperform the other two systems in power saving for high-agility maneuvers. Utilizing the advantages of less reaction, power saving and torque amplification for CMGs, Carpenter and Peck designed a three-link mechanism for agile coelostat telescope with each link actuated by a scissored pair of CMGs,[11] and investigated power-optimal control of the system.[12,13] Refs.[14–16] presented further researches on power and energy consumption of similar system.

It is noticeable that all the reactionless systems mentioned above use one-DOF free joint as link connection. Since the joint is free, it is possible to use three-DOF ball joint to replace the one-DOF joint so that more DOF of the end effector/payload can be obtained using less joints. Such design concept has been proposed recently,[17,18] and the results in Ref.[17] verified the advantages of the system on increasing the DOF of the end effector/payload and decreasing the system dynamical coupling. Trajectory tracking control approaches were also presented in Refs.[17,18], but the control laws were based on accurate system dynamics and no system uncertainty was taken into consideration. However, uncertainties of space robot systems, such as unknown disturbances, inertia parameter uncertainty and nonlinearity uncertainty, are almost inevitable in practical use. Therefore, a robust control law against system uncertainties is required to accomplish the control mission. Sliding mode control (SMC) is considered to be an effective strategy for control of uncertain systems, and has been widely applied to robotic systems.[19–21] Conventional SMC design usually requires a priori knowledge of the upper bound on the model uncertainty; however, such a bound may not be easily determined or estimated due to the complexity of the uncertainty structure. To solve the problem, the adaptive sliding mode control (ASMC) was proposed. Yoo and Chung,[22] and Leung et al.[23] proposed sliding mode controllers in which the control gains were tuned by integral-form adaptation laws designed to estimate the upper bound of the matched uncertainty, and smoothed the controller by introducing a boundary layer to alleviate chattering. Later, Wheeler et al.[24] pointed out that the control gains in Refs.[22,23] may grow infinite in the boundary layer because the ideal sliding surface cannot always be achieved. To overcome the drawback, he improved the adaptation laws to guarantee the boundedness of both the states and estimated control gains. Besides the integral-form adaptation laws, some other algorithms such as fuzzy algorithm[25] and artificial neural network,[26] were also applied to adapt the control gain. In recent years, many approaches have been proposed to improve the performance of the ASMC, for example, the methodologies designed to reduce the overestimation of the control gain,[27,28] and the adaptive high-order sliding mode controllers aimed at low chattering and finite-time convergence.[29,30]

The objective of this paper is to propose a robust controller for the ball-joint-connected space robot actuated by CMGs. Equations of motion are firstly derived using Kane's equations for a chain-configuration space robot system with arbitrary given number of joints. Dynamics analysis shows that for the rotational motion of each link or the base, the influences of various types of uncertainties can be classified as a "lumped" matched uncertainty with unknown upper bound. Then, inspired by Ref.[24], an ASMC law is proposed which guarantees uniformly ultimate boundedness of the closed loop system. The proposed controller not only inherits the advantages of chattering free response and finite control gains from Ref.[24], but also holds the following improvements: (1) in Ref.[24], it is assumed that the model uncertainty is bounded by a linear function of the state norm, and in this paper, the linear function is extended to a polynomial function of the state norm with arbitrary given order. This expands the application scope of the controller, especially for the systems with heavy nonlinear uncertainties; (2) a general amplification function is designed and incorporated in the adaptation law, and the necessary conditions of the amplification function are also presented explicitly. The function increases the estimation sensitivity within a small given range around the sliding surface, and therefore it can reduce the control error without increasing the control input magnitude evidently. Finally, simulation results and comparison are presented to demonstrate the effectiveness of the proposed controller.

## 2. System description

Fig. 1 shows the space robot studied in this paper. The system consists of $n$ rigid bodies (a base and $n-1$ links) which are connected by $n-1$ free ball joints. Each joint has three rotational DOF. A cluster (no less than three) of CMGs is installed on each body to actuate the system. The base is denoted as $B_1$, and the links are denoted as $B_2, B_3, \ldots, B_n$ (the links are numbered outward from the base). The joint which connects $B_i$ and its inner body is numbered as joint $i$. We denote $n_i$ as the number of CMGs installed on $B_i$, and call the $n_i$ CMGs as the $i$th cluster of CMGs.
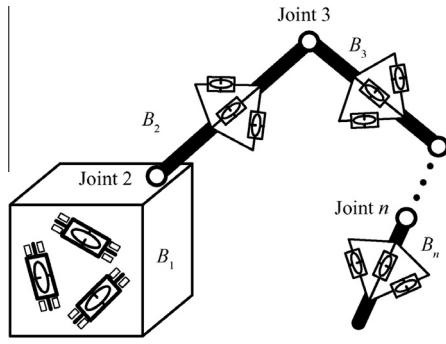
**Fig. 1**    Space robot actuated by CMGs.

For the proposed system, we make the following assumptions.

**Assumption 1.** The position of the mass center of each CMG does not change as the CMG rotates about its gimbal axis, so the total first moment of $B_i$ (including the CMGs on $B_i$, $i = 1, 2, \ldots, n$) is constant in any body-fixed coordinate of $B_i$.

**Assumption 2.** The variation of the total moment of inertia for $B_i$ (including the CMGs on $B_i$, $i = 1, 2, \ldots, n$) due to the rotation of the CMGs on $B_i$ is small, so it can be ignored, i.e., the total moment of inertia of $B_i$ is constant in any body-fixed coordinate of $B_i$.

From the view of robotic system level, the system can be regarded as a multibody system consisting of $n$ moving bodies (the base and the links), and each cluster of CMGs can be considered as a part of the corresponding moving body. In the sequel, unless specified, $B_i$ refers to the moving body plus the $i$th cluster of CMGs.

## 3. Equations of motion

### 3.1. System coordinates and basic vectors

In this section, we propose to develop the equations of motion of the system using Kane's equations. To describe the motion of the system, several coordinate systems are introduced as follows (see Fig. 2).

(1) Inertial coordinate system $F_0$ ($o_0$–$x_0 y_0 z_0$). The origin $o_0$ is located at an arbitrary point in inertial space, and the axes of $x_0$, $y_0$ and $z_0$ are fixed in the inertial space.
(2) The body-fixed coordinate system of the base, denoted as $F_1$ ($o_1$–$x_1 y_1 z_1$). The origin $o_1$ is located at an arbitrary
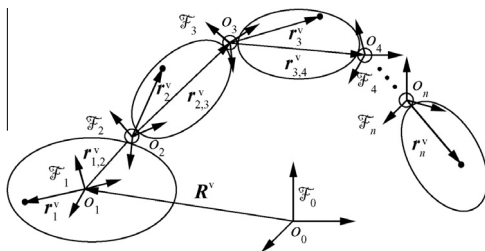


**Fig. 2**    Coordinate systems and position vectors.

point of $B_1$, and the axes of $x_1$, $y_1$ and $z_1$ are fixed in the base.
(3) The body-fixed coordinate system of the link $B_i$ ($i = 2, 3, \ldots, n$), denoted as $F_i$ ($o_i$–$x_i y_i z_i$). The origin $o_i$ is located at the center of the joint $i$, and the axes of $x_i$, $y_i$ and $z_i$ are fixed in $B_i$.

On the basis of the above coordinate systems, we denote $e_i = \left[ e_{ix}^{\mathrm{v}}, e_{iy}^{\mathrm{v}}, e_{iz}^{\mathrm{v}} \right]^{\mathrm{T}}$ ($i = 0, 1, \ldots, n$) as the vectrix[31] of $F_i$, where $e_{ix}^{\mathrm{v}}$, $e_{iy}^{\mathrm{v}}$ and $e_{iz}^{\mathrm{v}}$ are the directional unit vectors of the $x_i$, $y_i$ and $z_i$ axes of $F_i$, respectively. With the definition of the vectrices, an arbitrary three-dimensional vector $x^{\mathrm{v}}$ can be expressed as $x^{\mathrm{v}} = e_i^{\mathrm{T}} x$, where $x \in \mathbf{R}^3$ is the component column matrix of $x^{\mathrm{v}}$ in $F_i$. Given the definitions above, some vectors are defined as follows (see Fig. 2).

(1) $R^{\mathrm{v}} = e_0^{\mathrm{T}} R$, the position vector from $o_0$ to $o_1$, with $R \in \mathbf{R}^3$ the component column matrix of $R^{\mathrm{v}}$ in $F_0$.
(2) $r_i^{\mathrm{v}} = e_i^{\mathrm{T}} r_i$ ($i = 1, 2, \ldots, n$), the position vector from $o_i$ to a generic point in $B_i$, with $r_i \in \mathbf{R}^3$ the component column matrix of $r_i^{\mathrm{v}}$ in $F_i$.
(3) $r_{i,i+1}^{\mathrm{v}} = e_i^{\mathrm{T}} r_{i,i+1}$ ($i = 1, 2, \ldots, n$), the position vector from $o_i$ to $o_{i+1}$, with $r_{i,i+1} \in \mathbf{R}^3$ the component column matrix of $r_{i,i+1}^{\mathrm{v}}$ in $F_i$.
(4) $\omega_i^{\mathrm{v}} = e_i^{\mathrm{T}} \omega_i$ ($i = 1, 2, \ldots, n$), the angular velocity vector of $F_i$ with respect to $F_0$, with $\omega_i \in \mathbf{R}^3$ the component column matrix of $\omega_i^{\mathrm{v}}$ in $F_i$.

### 3.2. System kinematics

Since the links are connected by ball joints, we use the modified Rodrigues parameters (MRPs), instead of the traditional joint angles, to describe the angular displacements of the bodies. Denoting $\sigma_i = [\sigma_{i1}, \sigma_{i2}, \sigma_{i3}]^{\mathrm{T}}$ ($i = 1, 2, \ldots, n$) as the MRPs of $F_i$ with respect to $F_0$, we have[32–34]

$$\dot{\sigma}_i = H_i(\sigma_i)\omega_i \tag{1}$$

where

$$H_i(\sigma_i) = \frac{1}{2}\left[ I + \sigma_i^{\times} + \sigma_i \sigma_i^{\mathrm{T}} - \frac{1}{2}\left(1 + \sigma_i^{\mathrm{T}}\sigma_i\right)I \right] \tag{2}$$

with the superscript "×" the skew-symmetric cross product matrix of a $3 \times 1$ column matrix.

Choose the generalized speed matrix as

$$v = \left[ \dot{R}^{\mathrm{T}}, \ \omega_1^{\mathrm{T}}, \ \omega_2^{\mathrm{T}}, \ \ldots, \ \omega_n^{\mathrm{T}} \right]^{\mathrm{T}} \tag{3}$$

and the generalized displacement matrix as

$$q = \left[ R^{\mathrm{T}}, \ \sigma_1^{\mathrm{T}}, \ \sigma_2^{\mathrm{T}}, \ \ldots, \ \sigma_n^{\mathrm{T}} \right]^{\mathrm{T}} \tag{4}$$

then we obtain the kinematical equation of the system

$$\dot{q} = H(q)v \tag{5}$$

where

$$H(q) = \begin{bmatrix} I & \mathbf{0}_{3\times3} & \ldots & \mathbf{0}_{3\times3} \\ \mathbf{0}_{3\times3} & H_1 & \ldots & \mathbf{0}_{3\times3} \\ \vdots & \vdots & & \vdots \\ \mathbf{0}_{3\times3} & \mathbf{0}_{3\times3} & \ldots & H_n \end{bmatrix} \tag{6}$$

### 3.3. System dynamics

Now we begin to derive the dynamical equations of the system. The velocity of a generic point in $B_i$ ($i = 1, 2, \ldots, n$) can be written in the form of Eq. (7).

$$v_i^{\mathrm{v}} = e_1^{\mathrm{T}} G_i v \tag{7}$$

where $G_i \in \mathbf{R}^{3 \times (3n+3)}$ is the partial velocity matrix of the generic point in $B_i$, and given by the recursive expressions of Eq. (8).

$$\begin{cases} G_1 = \left[ A_{1,0}, -r_1^{\times}, \mathbf{0}_{3 \times (3n-3)} \right] \\ G_2 = \left[ A_{1,0}, -r_{1,2}^{\times}, -A_{1,2} r_2^{\times}, \mathbf{0}_{3 \times (3n-6)} \right] \\ \vdots \\ G_i = \left[ A_{1,0}, -r_{1,2}^{\times}, -A_{1,2} r_{2,3}^{\times}, -A_{1,3} r_{3,4}^{\times}, \ldots, -A_{1,i} r_i^{\times}, \mathbf{0}_{3 \times (3n-3i)} \right] \\ \vdots \\ G_n = \left[ A_{1,0}, -r_{1,2}^{\times}, -A_{1,2} r_{2,3}^{\times}, -A_{1,3} r_{3,4}^{\times}, \ldots, -A_{1,(n-1)} r_{n-1,n}^{\times}, -A_{1,n} r_n^{\times} \right] \end{cases} \tag{8}$$

where $A_{i,j} \in \mathbf{R}^{3 \times 3}$ represents the transform matrix from $F_j$ to $F_i$. The angular velocity of $B_i$ ($i = 1, 2, \ldots, n$) can also be written in the similar form to Eq. (7), that is,

$$\omega_i^{\mathrm{v}} = e_1^{\mathrm{T}} W_i v \tag{9}$$

where $W_i \in \mathbf{R}^{3 \times (3n+3)}$ is the partial angular velocity matrix of $B_i$, and given by

$$\begin{cases} W_1 = \left[ \mathbf{0}_{3 \times 3}, I, \mathbf{0}_{3 \times (3n-3)} \right] \\ W_2 = \left[ \mathbf{0}_{3 \times 6}, A_{1,2}, \mathbf{0}_{3 \times (3n-6)} \right] \\ \vdots \\ W_i = \left[ \mathbf{0}_{3 \times 3i}, A_{1,i}, \mathbf{0}_{3 \times (3n-3i)} \right] \\ \vdots \\ W_n = \left[ \mathbf{0}_{3 \times 3n}, A_{1,n} \right] \end{cases} \tag{10}$$

The acceleration vector of the generic point in $B_i$ can be obtained by taking time derivation of Eq. (7).

$$a_i^{\mathrm{v}} = e_1^{\mathrm{T}} G_i \dot{v} + e_1^{\mathrm{T}} \dot{G}_i v + e_1^{\mathrm{T}} \omega_1^{\times} G_i v \tag{11}$$

According to the Kane's equations in matrix form,[35] the generalized inertial force of the system can be evaluated by

$$F_{\mathrm{I}}^* = -\sum_{i=1}^{n} \int_{B_i} G_i^{\mathrm{T}} a_i^{\mathrm{l}} \mathrm{d}m = -M(q)\dot{v} - Q(q, v) \tag{12}$$

where $a_i^{\mathrm{l}}$ is the component column matrix of $a_i^{\mathrm{v}}$ in $F_1$; and

$$M(q) = \sum_{i=1}^{n} \int_{B_i} G_i^{\mathrm{T}} G_i \mathrm{d}m \tag{13}$$

is the positive definite mass matrix of the system, with $m$ the total mass of the system; and

$$Q(q, v) = \sum_{i=1}^{n} \int_{B_i} G_i^{\mathrm{T}} (\omega_1^{\times} G_i v + \dot{G}_i v) \mathrm{d}m \tag{14}$$

is the nonlinear inertial force matrix. The expressions of $M(q)$ and $Q(q, v)$ are given in Appendix A.

The active forces taken into consideration contain the following parts: (1) the control force acting on the base, denoted

as $F_1^{\mathrm{v}} = e_1^{\mathrm{T}} F_1^{\mathrm{l}}$ ($F_1^{\mathrm{l}}$ is the component column matrix of $F_1^{\mathrm{v}}$ in $F_1$); (2) the output torque of the $i$th cluster of CMGs acting on $B_i$ ($i = 1, 2, \ldots, n$), denoted as $T_{gi}^{\mathrm{v}} = e_1^{\mathrm{T}} T_{gi}^{\mathrm{l}}$ ($T_{gi}^{\mathrm{l}}$ is the component column matrix of $T_{gi}^{\mathrm{v}}$ in $F_1$); (3) the disturbance torque acting on $B_i$ ($i = 1, 2, \ldots, n$), denoted as $T_{di}^{\mathrm{v}} = e_1^{\mathrm{T}} T_{di}^{\mathrm{l}}$ ($T_{di}^{\mathrm{l}}$ is the component column matrix of $T_{di}^{\mathrm{v}}$ in $F_1$). Here we assume that the line of $F_1^{\mathrm{v}}$ passes through the point $o_1$, and then the active force matrix can be evaluated as

$$F_{\mathrm{A}}^* = (G_1^{o_1})^{\mathrm{T}} F_1^{\mathrm{l}} + \sum_{i=1}^{n} W_i^{\mathrm{T}} T_{gi}^{\mathrm{l}} + \sum_{i=1}^{n} W_i^{\mathrm{T}} T_{di}^{\mathrm{l}} \tag{15}$$

where $G_1^{o_1}$ is the partial velocity matrix of $o_1$, and given by

$$G_1^{o_1} = [A_{1,0}, \mathbf{0}_{3 \times 3n}] \tag{16}$$

Substituting Eqs. (10) and (16) into Eq. (15) yields

$$F_{\mathrm{A}}^* = \left[ F_1^{\mathrm{T}}, T_{g1}^{\mathrm{T}} + T_{d1}^{\mathrm{T}}, T_{g2}^{\mathrm{T}} + T_{d2}^{\mathrm{T}}, \ldots, T_{gn}^{\mathrm{T}} + T_{dn}^{\mathrm{T}} \right]^{\mathrm{T}} \tag{17}$$

where $F_1 = A_{0,1} F_1^{\mathrm{l}}$ is the component column matrix of $F_1^{\mathrm{v}}$ in $F_0$; $T_{gi} = A_{i,1} T_{gi}^{\mathrm{l}}$ and $T_{di} = A_{i,1} T_{di}^{\mathrm{l}}$ are the component column matrices of $T_{gi}^{\mathrm{v}}$ and $T_{di}^{\mathrm{v}}$ in $F_i$, respectively.

For a cluster of variable speed control moment gyroscopes (VSCMGs), $T_{gi}$ can be expressed as[36]

$$\begin{aligned} T_{gi} = &-A_{gi} I_{cgi} \ddot{\gamma}_i - A_{ti} I_{wsi} [\Omega_i]^{\mathrm{d}} \dot{\gamma}_i - A_{si} I_{wsi} \dot{\Omega}_i \\ &- \omega_i^{\times} (A_{gi} I_{cgi} \dot{\gamma}_i + A_{si} I_{wsi} \Omega_i) \end{aligned} \tag{18}$$

where $\gamma_i = [\gamma_{i1}, \gamma_{i2}, \ldots, \gamma_{in_i}]^{\mathrm{T}} \in \mathbf{R}^{n_i}$ and $\Omega_i = [\Omega_{i1}, \Omega_{i2}, \ldots, \Omega_{in_i}]^{\mathrm{T}} \in \mathbf{R}^{n_i}$ are column matrices whose elements are the gimbal angles and the rotor spin rates of the $i$th cluster of CMGs, respectively; $A_{gi}$, $A_{si}$ and $A_{ti}$ are $3 \times n_i$ matrices, whose columns are the component column matrices of the gimbal, rotor spin and transverse directional unit vectors in $F_i$, respectively; $I_{cgi} \in \mathbf{R}^{n_i \times n_i}$ is a diagonal matrix, whose elements are the moments of inertia of the whole CMGs (gimbal plus rotor) about the gimbal axes; $I_{wsi} \in \mathbf{R}^{n_i \times n_i}$ is a diagonal matrix whose elements are the moments of inertia of the rotors about the rotor spin axes; $[\Omega_i]^{\mathrm{d}} \in \mathbf{R}^{n_i \times n_i}$ is a diagonal matrix given by

$$[\Omega_i]^{\mathrm{d}} = \mathrm{diag} \left( \Omega_{i1}, \Omega_{i2}, \ldots, \Omega_{in_i} \right) \tag{19}$$

In this study, we only consider using constant speed CMGs, and hence the term $A_{si} I_{wsi} \dot{\Omega}_i$ in Eq. (18) can be eliminated. Generally, the gimbal acceleration term $A_{gi} I_{cgi} \ddot{\gamma}_i$ is small enough to be ignored;[37] moreover, the angular momentum of the gimbal velocity term $A_{gi} I_{cgi} \dot{\gamma}_i$ is small in comparison with the term $A_{si} I_{wsi} \Omega_i$, so it can also be ignored.[38] Therefore, $T_{gi}$ can be simplified as

$$T_{gi} = -A_{ti} I_{wsi} [\Omega_i]^{\mathrm{d}} \dot{\gamma}_i - \omega_i^{\times} A_{si} I_{wsi} \Omega_i \tag{20}$$

We reasonably assume that the rotors of the CMGs in the $i$th cluster have the same magnitude of angular momentum, denoted as $h_i$. Given this, Eq. (20) can be written as

$$T_{gi} = -h_i A_{ti} \dot{\gamma}_i - \omega_i^{\times} A_{si} h_i \tag{21}$$

where

$$h_i = I_{wsi} \Omega_i = \underbrace{[h_i, h_i, \ldots, h_i]}_{n_i}^{\mathrm{T}} \tag{22}$$

According to the Kane's equations in matrix form,[35] the dynamical equation of the system can be written in the form of Eq. (23).

$$F_I^* + F_A^* = 0 \tag{23}$$

Substituting Eqs. (12) and (17) into Eq. (23), we can arrange the dynamical equation as

$$M(q)\dot{v} + Q(q, v) = F_c + F_d \tag{24}$$

where

$$F_c = \left[ F_1^T, T_{g1}^T, T_{g2}^T, \dots, T_{gn}^T \right]^T \tag{25}$$

$$F_d = \left[ 0_{3\times1}^T, T_{d1}^T, T_{d2}^T, \dots, T_{dn}^T \right]^T \tag{26}$$

The dynamical Eq. (24) and the kinematical Eq. (5) together constitute the governing equations of motion of the system, and can be used for dynamical simulation, as well as the basis of system controller design.

## 4. Control problem statement

In general, the control objective of a space robot is to drive the manipulator variables to track their desired trajectories. Without loss of generality, here the manipulator variable is defined as

$$\Psi = \left[ R^T, \quad \sigma_1^T, \quad R_n^T, \quad \sigma_n^T \right]^T \tag{27}$$

where $R_n$ is the position of the end effector/payload (the tip body of the multibody system); $\Psi$ is related to system displacement $q$ by Jacobian matrix $J(q)$ as

$$\dot{\Psi} = J(q)\dot{q} \tag{28}$$

Denote $\Psi_d(t)$ as the desired trajectory of the manipulator variable $\Psi$, and $q_d = \left[ R_d^T, \sigma_{1d}^T, \sigma_{2d}^T, \dots, \sigma_{nd}^T \right]^T$ as the desired value of $q$, then $\dot{q}_d$ and $\ddot{q}_d$ can be derived as

$$\dot{q}_d = J^+(q_d)\dot{\Psi}_d(t) \tag{29}$$

$$\ddot{q}_d = J^+(q_d)\ddot{\Psi}_d(t) + \dot{J}^+(q_d)\dot{\Psi}_d(t) \tag{30}$$

where $J^+(q_d) = J^T(q_d)(J(q_d)J^T(q_d))^{-1}$ is the pseudoinverse of $J(q_d)$. Given $\dot{q}_d$, $q_d$ can be acquired using time integral of $\dot{q}_d$. Since $\Psi_d(t)$ is supposed to be a function of $t$, $q_d$ is also a function of $t$ and can be written as $q_d(t)$.

From the view of practical application, in this study, the base position $R$ is not supposed to be controlled during the manipulator operation. To this end, the current $R$, $\dot{R}$ and $\ddot{R}$ are used for the desired variables $R_d(t)$, $\dot{R}_d(t)$ and $\ddot{R}_d(t)$, respectively, and the control force $F_1$ is set to be zero. Such method was also used by Senda and Nagaoka to address similar problems.[39] The control objective is to drive $\sigma_i (i = 1, 2, \dots, n)$ to track its desired trajectory $\sigma_{id}(t)$. We propose to design the control system using decentralized approach, in which the controller of $\sigma_i$ is to be designed separately from those of $\sigma_j (j \neq i)$. Therefore, it is necessary to separately investigate the governing rotational dynamical equation of $B_i$, which can be extracted from Eq. (24) and arranged in the form of

$$M_i \dot{\omega}_i + F_{M_i}(\cdot) + Q_i(q, v) = T_{gi} + T_{di} \tag{31}$$

where $M_i \in \mathbf{R}^{3\times3}$ is the corresponding diagonal partition matrix of $M(q)$, which is a constant matrix (see Appendix A); $Q_i(q, u)$ is the corresponding partition column matrix of $Q(q, v)$; $F_{M_i}(\cdot)$ is given by

$$F_{M_i}(\cdot) = M_{i0}(q)\ddot{R} + \sum_{j=1}^{i-1} M_{ij}(q)\dot{\omega}_j + \sum_{j=i+1}^{n} M_{ij}(q)\dot{\omega}_j \tag{32}$$

where $M_{ij}(q)(j = 0, 1, \dots, i-1, i+1, \dots, n)$ is the corresponding non-diagonal partition matrix of $M(q)$. Explicitly, $F_{M_i}(\cdot)$ represents the direct disturbance torque of the other bodies acting on $B_i$.

From Eq. (1), we know that

$$\begin{cases} \omega_i = H_i^{-1}(\sigma_i)\dot{\sigma}_i \\ \dot{\omega}_i = H_i^{-1}(\sigma_i)\ddot{\sigma}_i + \dot{H}_i^{-1}(\sigma_i)\dot{\sigma}_i \end{cases} \tag{33}$$

Inserting Eq. (33) into Eq. (31) and left multiplying the resulting equation by $H_i^{-T}(\sigma_i)$ yield

$$M_i^*(\sigma_i)\ddot{\sigma}_i = H_i^{-T}(\sigma_i)T_{gi} + H_i^{-T}(\sigma_i)T_{Di}(\sigma_i, \dot{\sigma}_i) \tag{34}$$

where $M_i^*(\sigma_i) = H_i^{-T}(\sigma_i)M_i H_i^{-1}(\sigma_i)$ is the symmetric "modified" mass matrix, and

$$T_{Di}(\sigma_i, \dot{\sigma}_i) = T_{di} - M_i \dot{H}(\sigma_i)_i^{-1}\dot{\sigma}_i - F_{M_i}(\cdot) - Q_i(q, v) \tag{35}$$

Considering the uncertainty of the inertial parameters, the mass matrix $M_i^*(\sigma_i)$ can be divided into two parts, that is, $M_i^*(\sigma_i) = M_{i0}^*(\sigma_i) + \Delta M_i^*(\sigma_i)$, where the first part $M_{i0}^*(\sigma_i)$ is evaluated using the nominal inertial parameters, and the second part $\Delta M_i^*(\sigma_i)$ is the uncertain part. Given this, Eq. (34) can be rearranged in the form of Eq. (36).

$$\ddot{\sigma}_i = \bar{u}_i + \bar{d}_i(\sigma_i, \dot{\sigma}_i) \tag{36}$$

where

$$\bar{u}_i = \left[ M_{i0}^*(\sigma_i) \right]^{-1} H_i^{-T}(\sigma_i)T_{gi} \tag{37}$$

and

$$\bar{d}_i(\sigma_i, \dot{\sigma}_i) = \left[ M_i^*(\sigma_i) \right]^{-1} H_i^{-T}(\sigma_i)T_{Di}(\sigma_i, \dot{\sigma}_i) + \left( \left[ M_i^*(\sigma_i) \right]^{-1} M_{i0}^*(\sigma_i) - I \right)\bar{u}_i \tag{38}$$

Now we define

$$\Delta\sigma_i = \sigma_i - \sigma_{id}(t) \tag{39}$$

as the tracking error of $\sigma_i$ and

$$x_i = \begin{bmatrix} \Delta\sigma_i \\ \Delta\dot{\sigma}_i \end{bmatrix} \tag{40}$$

as system state, and then Eq. (36) can be written in the state equation form of

$$\dot{x}_i = A_i x_i + B_i(u_i + d_i(x_i, t)) \tag{41}$$

where $A_i = \begin{bmatrix} 0_{3\times3} & I \\ 0_{3\times3} & 0_{3\times3} \end{bmatrix}$ and $B_i = \begin{bmatrix} 0_{3\times3} \\ I \end{bmatrix}$ are constants.

$$u_i = \bar{u}_i - \ddot{\sigma}_{id}(t) \tag{42}$$

is taken as system control input, and

$$d_i(x_i, t) = \bar{d}_i(\sigma_i, \dot{\sigma}_i) \tag{43}$$

is the "lumped" uncertainty including the uncertainties of inertial parameters, system nonlinearity and unknown disturbances. To be strict, part of $d_i(x_i, t)$ can be precisely

evaluated using the measurements of $\boldsymbol{\sigma}_i$ and $\boldsymbol{\omega}_i$ (for example, part of the system nonlinear term) despite the initial parameter uncertainty, and hence the part can be treated as known quantity in controller design. However, in order to simplify the controller algorithm, as well as to reduce the dependence of the controller design on system dynamical model, the whole term of $\boldsymbol{d}_i(\boldsymbol{x}_i, t)$ is still taken as uncertainty.

By now, the control problem becomes clear, that is, seeking for proper control input $\boldsymbol{u}_i$ for system Eq. (41) to drive $\boldsymbol{x}_i \rightarrow \boldsymbol{0}$ under the disturbance of the "lumped" uncertainty $\boldsymbol{d}_i(\boldsymbol{x}_i, t)$.

## 5. Control law design

To complete the description of system Eq. (41), we state the following assumptions. For convenience, in this section, the subscript "$i$" is omitted.

**Assumption 3.** The pair $(\boldsymbol{A}, \boldsymbol{B})$ is completely controllable.

**Assumption 4.** The uncertainty $\boldsymbol{d}(\boldsymbol{x}, t)$ is continuous on its arguments.

**Remark 1.** Assumption 3 is distinctly valid for system Eq. (41). However, if the uncertainty $\boldsymbol{d}(\boldsymbol{x}, t)$ contains joint friction torques, Assumption 4 may be called in question, because in some rough models the friction is discontinuous. But in accurate models which consider many aspects of friction such as stiction, stick–slip, Stribeck, etc., friction is indeed continuous.[40] Therefore, Assumption 4 is also valid for system Eq. (41) in theory, although sometimes (especially when the friction direction is being changed) the friction behaves like discontinuous force and hence worsens system performance.

Since we propose to design the controller using SMC method, we begin with the first phase of a sliding surface construction so that the system restricted to the sliding surface produces desired behavior.[41] The resulting sliding surface is given by

$$\boldsymbol{\Theta} = \{\boldsymbol{x} : \boldsymbol{S}(\boldsymbol{x}) = \boldsymbol{C}\boldsymbol{x} = \boldsymbol{0}\} \tag{44}$$

where $\boldsymbol{C} \in \mathbf{R}^{3 \times 6}$ is a constant matrix whose elements are chosen on the basis of the desired behavior. Here we assume that $\boldsymbol{C}$ is of full rank and the matrix $\boldsymbol{CB}$ is nonsingular.

After the sliding surface selection, the next phase is to design the control law so that the condition $\boldsymbol{S}^{\mathrm{T}}\dot{\boldsymbol{S}} < \boldsymbol{0}$ is satisfied. This condition guarantees that the system trajectories reach the sliding surface and remain there for all subsequent time. The character of the "lumped" uncertainty $\boldsymbol{d}(\boldsymbol{x}, t)$, as the open literature has shown, has prominent effect on the control law design. If we can find a continuous positive scalar valued function $\rho(\boldsymbol{x}, t)$, such that $\|\boldsymbol{d}(\boldsymbol{x}, t)\| \leqslant \rho(\boldsymbol{x}, t)$ for all $(\boldsymbol{x}, t) \in \mathbf{R}^6 \times \mathbf{R}$, then an SMC law guaranteeing $\boldsymbol{S}^{\mathrm{T}}\dot{\boldsymbol{S}} < \boldsymbol{0}$ can be developed using the results in Ref.[41]. However, for the system studied in this paper, such a function $\rho(\boldsymbol{x}, t)$ is not easy to be obtained, that is, the upper bound of the norm $\|\boldsymbol{d}(\boldsymbol{x}, t)\|$ is uncertain. To handle this problem, Yoo and Chung[22] proposed the adaptation laws which are capable of estimating the upper bound of the norm $\|\boldsymbol{d}(\boldsymbol{x}, t)\|$, and designed a SMC law using the estimated upper bound. The control scheme in Ref.[22] is based on the assumption below.

**Assumption 5.** There are positive constants, $c_0$ and $c_1$, such that $\|\boldsymbol{d}(\boldsymbol{x}, t)\| \leqslant c_0 + c_1\|\boldsymbol{x}\| = \rho(\boldsymbol{x}, t)$ for all $(\boldsymbol{x}, t) \in \mathbf{R}^6 \times \mathbf{R}$.

The control law proposed by Yoo and Chung[22] is given by

$$\boldsymbol{u} = -(\boldsymbol{CB})^{-1}\boldsymbol{K}_{\mathrm{D}}\boldsymbol{S} + \boldsymbol{u}_{\mathrm{eq_{nom}}} + \boldsymbol{u}_{\mathrm{N}} \tag{45}$$

where $\boldsymbol{K}_{\mathrm{D}} \in \mathbf{R}^{3 \times 3}$ is a positive definite matrix; $\boldsymbol{u}_{\mathrm{eq_{nom}}}$ is the equivalent control for the nominal system of Eq. (41) by assuming that the uncertainty $\boldsymbol{d}(\boldsymbol{x}, t)$ is zero, and determined by

$$\boldsymbol{u}_{\mathrm{eq_{nom}}} = -(\boldsymbol{CB})^{-1}\boldsymbol{CAx} \tag{46}$$

The term $\boldsymbol{u}_{\mathrm{N}}$ is the nonlinear feedback control for suppression of the effect of the uncertainty, and defined as

$$\boldsymbol{u}_{\mathrm{N}} = \begin{cases} -\dfrac{\boldsymbol{B}^{\mathrm{T}}\boldsymbol{C}^{\mathrm{T}}\boldsymbol{S}}{\|\boldsymbol{B}^{\mathrm{T}}\boldsymbol{C}^{\mathrm{T}}\boldsymbol{S}\|}\bar{\rho}(\boldsymbol{x}, t) & \boldsymbol{S} \neq \boldsymbol{0} \\ \boldsymbol{0} & \boldsymbol{S} = \boldsymbol{0} \end{cases} \tag{47}$$

where $\bar{\rho}(\boldsymbol{x}, t)$ is the adaptive upper bound of $\|\boldsymbol{d}(\boldsymbol{x}, t)\|$ and evaluated by

$$\bar{\rho}(\boldsymbol{x}, t) = \bar{c}_0 + \bar{c}_1\|\boldsymbol{x}\| \tag{48}$$

Therein, $\bar{c}_0$ and $\bar{c}_1$ are the estimated values of $c_0$ and $c_1$, respectively, and given by the adaptation laws of Eq. (49).

$$\begin{cases} \dot{\bar{c}}_0 = q_0\|\boldsymbol{B}^{\mathrm{T}}\boldsymbol{C}^{\mathrm{T}}\boldsymbol{S}\| \\ \dot{\bar{c}}_1 = q_1\|\boldsymbol{B}^{\mathrm{T}}\boldsymbol{C}^{\mathrm{T}}\boldsymbol{S}\|\|\boldsymbol{x}\| \end{cases} \tag{49}$$

where $q_0$ and $q_1$ are adaptation gains with positive values. Yoo and Chung have proved that for system Eq. (41), if Assumptions 3–5 are valid, $\boldsymbol{S} = \boldsymbol{0}$ is asymptotically stable by employing the control law Eq. (45) with $\boldsymbol{u}_{\mathrm{N}}$ given in Eq. (47). By analyzing the structure of $\boldsymbol{u}_{\mathrm{N}}$, Yoo and Chung also pointed out that the undesirable chattering phenomenon may occur due to the discontinuity of $\boldsymbol{u}_{\mathrm{N}}$ at $\boldsymbol{S} = \boldsymbol{0}$, and therefore they took a further step to modify $\boldsymbol{u}_{\mathrm{N}}$ as[22]

$$\boldsymbol{u}_{\mathrm{N}} = \begin{cases} -\dfrac{\boldsymbol{B}^{\mathrm{T}}\boldsymbol{C}^{\mathrm{T}}\boldsymbol{S}}{\|\boldsymbol{B}^{\mathrm{T}}\boldsymbol{C}^{\mathrm{T}}\boldsymbol{S}\|}\bar{\rho}(\boldsymbol{x}, t) & \|\boldsymbol{B}^{\mathrm{T}}\boldsymbol{C}^{\mathrm{T}}\boldsymbol{S}\| > \varepsilon \\ -\dfrac{\boldsymbol{B}^{\mathrm{T}}\boldsymbol{C}^{\mathrm{T}}\boldsymbol{S}}{\varepsilon}\bar{\rho}(\boldsymbol{x}, t) & \|\boldsymbol{B}^{\mathrm{T}}\boldsymbol{C}^{\mathrm{T}}\boldsymbol{S}\| \leqslant \varepsilon \end{cases} \tag{50}$$

where $\bar{\rho}(\boldsymbol{x}, t)$ and the adaptation laws are still given by Eqs. (48) and (49); $\varepsilon$ is the boundary layer parameter, and usually chosen as a small positive value. Though the control law with $\boldsymbol{u}_{\mathrm{N}}$ given in Eq. (50) loses asymptotic stability, the performance can be made arbitrarily close to that of the original control law in which $\boldsymbol{u}_{\mathrm{N}}$ is given by Eq. (47).

Later, Wheeler et al.[24] found that for the control law Eq. (45) with $\boldsymbol{u}_{\mathrm{N}}$ given in Eq. (50), the estimated gains $\bar{c}_0$ and $\bar{c}_1$ determined by Eq. (49) may become unbounded in the boundary layer since the restriction to the sliding surface cannot always be achieved precisely. To eliminate the drawback, they modified $\boldsymbol{u}_{\mathrm{N}}$ and the adaptation laws as

$$\boldsymbol{u}_{\mathrm{N}} = \begin{cases} -\dfrac{\boldsymbol{B}^{\mathrm{T}}\boldsymbol{C}^{\mathrm{T}}\boldsymbol{S}}{\|\boldsymbol{B}^{\mathrm{T}}\boldsymbol{C}^{\mathrm{T}}\boldsymbol{S}\|}\bar{\rho}(\boldsymbol{x}, t) & \bar{\rho}(\boldsymbol{x}, t)\|\boldsymbol{B}^{\mathrm{T}}\boldsymbol{C}^{\mathrm{T}}\boldsymbol{S}\| > \varepsilon \\ -\dfrac{\boldsymbol{B}^{\mathrm{T}}\boldsymbol{C}^{\mathrm{T}}\boldsymbol{S}}{\varepsilon}\bar{\rho}^2(\boldsymbol{x}, t) & \bar{\rho}(\boldsymbol{x}, t)\|\boldsymbol{B}^{\mathrm{T}}\boldsymbol{C}^{\mathrm{T}}\boldsymbol{S}\| \leqslant \varepsilon \end{cases} \tag{51}$$

$$\bar{\rho}(\boldsymbol{x}, t) = \bar{c}_0 + \bar{c}_1\|\boldsymbol{x}\| \tag{52}$$

$$\begin{cases} \dot{\bar{c}}_0 = q_0\left(-\psi_0\bar{c}_0 + \|\boldsymbol{B}^{\mathrm{T}}\boldsymbol{C}^{\mathrm{T}}\boldsymbol{S}\|\right) \\ \dot{\bar{c}}_1 = q_1\left(-\psi_1\bar{c}_1 + \|\boldsymbol{B}^{\mathrm{T}}\boldsymbol{C}^{\mathrm{T}}\boldsymbol{S}\|\|\boldsymbol{x}\|\right) \end{cases} \tag{53}$$

where $\psi_0$ and $\psi_1$ are constants chosen by the designer. Wheeler et al.[24] have proved that if Assumptions 3–5 are valid, then the control law Eq. (45) with $\boldsymbol{u}_{\mathrm{N}}$ in Eq. (51) is continuous and in the closed loop system $\boldsymbol{S}(\boldsymbol{x})$ and all signals are uniformly ultimately bounded. However, direct application of Wheeler's control law to the system studied in this paper may arouse two problems. The first one is about the Assumption 5. Since the "lumped" uncertainty $\boldsymbol{d}(\boldsymbol{x}, t)$ contains complex nonlinearities, maybe the Assumption 5 is no more valid. The second one is about the control law itself. Though the system is proved to be uniformly ultimately bounded, there is no sufficient evidence showing $\bar{c}_0 \geqslant c_0$ and $\bar{c}_1 \geqslant c_1$ for all $(\boldsymbol{x}, t)$, which implies there exists the possibility of $\bar{\rho}(\boldsymbol{x}, t) \leqslant \rho(\boldsymbol{x}, t)$. When $\bar{\rho}(\boldsymbol{x}, t) \leqslant \rho(\boldsymbol{x}, t)$, the control error may increase. The possibility of $\bar{\rho}(\boldsymbol{x}, t) \leqslant \rho(\boldsymbol{x}, t)$ increases when $\|\boldsymbol{S}\| \to 0$ because $\dot{\bar{c}}_0$ and $\dot{\bar{c}}_1$ may be negative, and hence $\bar{\rho}(\boldsymbol{x}, t)$ may decrease at this point. Therefore, we hope to increase $\bar{\rho}(\boldsymbol{x}, t)$ when $\|\boldsymbol{S}\|$ enters a neighborhood of zero to reduce the possibility of $\bar{\rho}(\boldsymbol{x}, t) \leqslant \rho(\boldsymbol{x}, t)$ and consequently reduce the control error. Motivated by the above two problems, we first expand Assumption 5 to Assumption 6 as shown below.

**Assumption 6.** There are positive constants, $c_0$, $c_1, \ldots, c_N$, where $N$ is a given positive integer, such that $\|\boldsymbol{d}(\boldsymbol{x}, t)\| \leqslant c_0 + c_1\|\boldsymbol{x}\| + \ldots + c_N\|\boldsymbol{x}\|^N = \rho(\boldsymbol{x}, t)$ for all $(\boldsymbol{x}, t) \in \mathbf{R}^6 \times \mathbf{R}$.

Based on Assumption 6, we then modify $\boldsymbol{u}_{\mathrm{N}}$ as

$$\boldsymbol{u}_{\mathrm{N}} = \begin{cases} -\dfrac{\boldsymbol{B}^{\mathrm{T}}\boldsymbol{C}^{\mathrm{T}}\boldsymbol{S}}{\|\boldsymbol{B}^{\mathrm{T}}\boldsymbol{C}^{\mathrm{T}}\boldsymbol{S}\|^2}P\left(\|\boldsymbol{B}^{\mathrm{T}}\boldsymbol{C}^{\mathrm{T}}\boldsymbol{S}\|\right)\bar{\rho} & \bar{\rho}\|\boldsymbol{B}^{\mathrm{T}}\boldsymbol{C}^{\mathrm{T}}\boldsymbol{S}\|^2 > \varepsilon P\left(\|\boldsymbol{B}^{\mathrm{T}}\boldsymbol{C}^{\mathrm{T}}\boldsymbol{S}\|\right) \\[2mm] -\dfrac{\boldsymbol{B}^{\mathrm{T}}\boldsymbol{C}^{\mathrm{T}}\boldsymbol{S}}{\varepsilon}\bar{\rho}^2 & \bar{\rho}\|\boldsymbol{B}^{\mathrm{T}}\boldsymbol{C}^{\mathrm{T}}\boldsymbol{S}\|^2 \leqslant \varepsilon P\left(\|\boldsymbol{B}^{\mathrm{T}}\boldsymbol{C}^{\mathrm{T}}\boldsymbol{S}\|\right) \end{cases} \tag{54}$$

where $P(\bullet)$ is a scalar function. For any $x \geqslant 0$, the function $P(x)$ in Eq. (54) is defined as

$$P(x) = \begin{cases} g(x) & x \leqslant \delta \\ x & x > \delta \end{cases} \tag{55}$$

Therein, $\delta > 0$ is a constant; $g(x)$ is a scalar continuous function chosen by the designer which satisfies the following conditions.
**Condition 1**

(1) $g(0) = 0$, $g(\delta) = \delta$. This condition guarantees the continuity of $\boldsymbol{u}_{\mathrm{N}}$.
(2) $g(x) > x$, for $x \in (0, \delta)$. This condition ensures $P(x) \geqslant x$ for all $x \geqslant 0$, and hence the control error is reduced.
(3) There is a positive constant $\kappa$, such that $\kappa = \max\left(\dfrac{g(x)}{x}\right)$. This condition guarantees the stability of the closed loop system (see Appendix B).

In Eq. (54), $\bar{\rho}(\boldsymbol{x}, t)$ is given by

$$\bar{\rho}(\boldsymbol{x}, t) = \bar{c}_0 + \bar{c}_1\|\boldsymbol{x}\| + \ldots + \bar{c}_N\|\boldsymbol{x}\|^N \tag{56}$$

where $\bar{c}_0$, $\bar{c}_1, \ldots, \bar{c}_N$ are the estimated values of $c_0$, $c_1, \ldots, c_N$, respectively, and evaluated by the adaptation laws of Eq. (57).

$$\begin{cases} \dot{\bar{c}}_0 = q_0\left[-\psi_0\bar{c}_0 + P\left(\|\boldsymbol{B}^{\mathrm{T}}\boldsymbol{C}^{\mathrm{T}}\boldsymbol{S}\|\right)\right] \\ \dot{\bar{c}}_1 = q_1\left[-\psi_1\bar{c}_1 + P\left(\|\boldsymbol{B}^{\mathrm{T}}\boldsymbol{C}^{\mathrm{T}}\boldsymbol{S}\|\right)\|\boldsymbol{x}\|\right] \\ \vdots \\ \dot{\bar{c}}_N = q_N\left[-\psi_N\bar{c}_N + P\left(\|\boldsymbol{B}^{\mathrm{T}}\boldsymbol{C}^{\mathrm{T}}\boldsymbol{S}\|\right)\|\boldsymbol{x}\|^N\right] \end{cases} \tag{57}$$

It can be proved that if Assumptions 3, 4 and 6 are valid, the closed loop system constructed using control law Eq. (45) with $\boldsymbol{u}_{\mathrm{N}}$ in Eq. (54) is uniformly ultimately bounded. The proof is presented in Appendix B.

**Remark 2.** Since the nonlinear terms are all treated as system uncertainty, the positive integer $N$ maybe cannot be chosen very precisely. To be conservative, $N$ can be chosen as a larger integer, because if the integer matching the real system (denoted as $N_{\mathrm{r}}$) is smaller than the selected integer $N$, Assumption 6 is still valid by letting $c_k = 0$ ($k = N_{\mathrm{r}} + 1$, $N_{\mathrm{r}} + 2, \ldots, N$). However, if $N_{\mathrm{r}} > N$, the Assumption 6 is no more valid.

**Remark 3.** The purpose of the introduction of $P(x)$ is to amplify the estimated $\bar{\rho}(\boldsymbol{x}, t)$ in a predesigned interval of $\|\boldsymbol{B}^{\mathrm{T}}\boldsymbol{C}^{\mathrm{T}}\boldsymbol{S}\| \in (0, \delta)$ so as to reduce the control error. Generally, $\delta$ should be chosen as a small positive value, otherwise, the controller may take the risk of producing overlarge control input beyond the capacity of the actuators when $\|\boldsymbol{B}^{\mathrm{T}}\boldsymbol{C}^{\mathrm{T}}\boldsymbol{S}\|$ is far from zero. In Wheeler's control law and adaption law, the control error can also be reduced by increasing $q_0$ and $q_1$ and decreasing $\psi_0$ and $\psi_1$, but with the same risk as mentioned above. In a word, we expect control error reduction at the cost of few increase of control input.

## 6. Steering law for CMGs

Once the control input $\boldsymbol{u}_i$ is obtained by the control law, the desired value of the CMG torque $\boldsymbol{T}_{gi}$, denoted as $\boldsymbol{T}_{\mathrm{d}gi}$, can be uniquely determined using Eqs. (37) and (42) as given below.

$$\boldsymbol{T}_{\mathrm{d}gi} = \boldsymbol{H}^{\mathrm{T}}(\boldsymbol{\sigma}_i)\boldsymbol{M}_{i0}^*(\boldsymbol{\sigma}_i)(\boldsymbol{u}_i + \ddot{\boldsymbol{\sigma}}_{\mathrm{d}i}(t)) \tag{58}$$

Based on Eq. (20), we know that to provide the desired torque $\boldsymbol{T}_{\mathrm{d}gi}$, the gimbal angular velocity of the $i$th cluster of CMGs, $\dot{\boldsymbol{\gamma}}_i$, must satisfy

$$\boldsymbol{T}_{\mathrm{d}gi} = -\boldsymbol{A}_{\mathrm{t}i}\boldsymbol{I}_{\mathrm{ws}i}[\boldsymbol{\Omega}_i]^{\mathrm{d}}\dot{\boldsymbol{\gamma}}_i - \boldsymbol{\omega}_i^\times\boldsymbol{A}_{\mathrm{s}i}\boldsymbol{I}_{\mathrm{ws}i}\boldsymbol{\Omega}_i \tag{59}$$

Here we assume $n_i \geqslant 4$ ($i = 1, 2, \ldots, n$). Because of the redundancy of the CMGs, there are infinite solutions of $\dot{\boldsymbol{\gamma}}_i$ satisfying Eq. (59). To avoid the configuration singularity, we use the well-developed steering law with null motion, that is,

$$\dot{\boldsymbol{\gamma}}_i = \dot{\boldsymbol{\gamma}}_{\mathrm{T}i} + \dot{\boldsymbol{\gamma}}_{\mathrm{N}i} \tag{60}$$

where

$$\dot{\boldsymbol{\gamma}}_{\mathrm{T}i} = -\frac{1}{h_i}\boldsymbol{A}_{\mathrm{t}i}^{\mathrm{T}}(\boldsymbol{A}_{\mathrm{t}i}\boldsymbol{A}_{\mathrm{t}i}^{\mathrm{T}})^{-1}(\boldsymbol{T}_{\mathrm{d}gi} + \boldsymbol{\omega}_i^\times\boldsymbol{A}_{\mathrm{s}i}\boldsymbol{I}_{\mathrm{ws}i}\boldsymbol{\Omega}_i) \tag{61}$$

is used to provide the desired control torque, and

$$\dot{\boldsymbol{\gamma}}_{\mathrm{N}i} = \alpha_i\left[\boldsymbol{I} - \boldsymbol{A}_{\mathrm{t}i}^{\mathrm{T}}(\boldsymbol{A}_{\mathrm{t}i}\boldsymbol{A}_{\mathrm{t}i}^{\mathrm{T}})^{-1}\boldsymbol{A}_{\mathrm{t}i}\right]\frac{\partial\eta_i}{\partial\boldsymbol{\gamma}_i} \tag{62}$$

is the null motion used to avoid the configuration singularity. Therein, $\alpha_i$ is a positive scalar parameter chosen by the designer, and $\eta_i = \det(A_{ti}A_{ti}^T)$ is the measurement of configuration singularity.

## 7. Numerical example

### 7.1. System configuration and parameters

The numerical example is concerned with a system containing a cubic base and three links. The length of side of the base is 1.5 m, the length of the link $B_2$ and $B_3$ is 1.5 m, and that of the link $B_4$ (the end effector/payload) is 0.6 m. The origin of $F_1$ is located at the geometrical center of the base, and the axes of $F_1$ are parallel to the edge lines of the cube. When the axes of $F_1$ are parallel to the corresponding axes of the body-fixed coordinates of the links, the system configuration is shown in Fig. 3(a). Different CMG configurations can be adopted to provide the control torques provided that $n_i \geqslant 4 \, (i = 1, 2, \ldots, n)$; nevertheless, we select the pyramid configuration due to its close-to-spherical angular momentum envelop, i.e., a cluster of CMGs arranged in pyramid configuration is installed on the base as well as each link. The centering axis of the pyramid is along the direction of the $z_i$ axis of $F_i$, and the gimbal axis of each CMG has the same included angle of $\beta = 53.1°$ with the centering axis (see Fig. 3(b), where $\dot{\gamma}_{ij}^v \, (j = 1, 2, 3, 4)$ and $h_{ij}^v \, (j = 1, 2, 3, 4)$ represent the gimbal angular velocity and rotor angular momentum of the $j$th CMG in $i$th cluster, respectively). Table 1 lists system inertial



(a) Configuration of base and links    (b) Configuration of CMGs

**Fig. 3**    Configuration of system in numerical example.

parameters. The moments of inertia and the first moments are evaluated based on the corresponding body-fixed coordinates. As the values of the first moments are unused in controller design, we merely need to present the true values.

The geometric parameters are

$$\begin{cases} r_{1,2} = [0, 0.75, 0.75]^T \text{ m} \\ r_{2,3} = r_{3,4} = [0, 0, 1.5]^T \text{ m} \end{cases}$$

The magnitudes of the angular momentums of the CMGs, $h_i \, (i = 1, 2, 3, 4)$, are chosen as

$$\begin{cases} h_1 = 100 \text{ N} \cdot \text{m} \cdot \text{s}, \quad h_2 = 50 \text{ N} \cdot \text{m} \cdot \text{s} \\ h_3 = 40 \text{ N} \cdot \text{m} \cdot \text{s}, \quad h_4 = 30 \text{ N} \cdot \text{m} \cdot \text{s} \end{cases}$$

The initial gimbal angles of the CMGs are chosen to be

$$\gamma_{i0} = [0, \quad 0, \quad 0, \quad 0]^T \, (°) \, (i = 1, 2, 3, 4)$$

When $\gamma_{i0} = [0, \quad 0, \quad 0, \quad 0]^T \, (°)$, the angular momentum vector of each CMG in the $i$th cluster will be parallel to the basal plane of the pyramid (see Fig. 3(b)). The initial system velocity $v_0 = 0$, and the initial system displacements in $q_0 = [R_0^T, \sigma_{10}^T, \sigma_{20}^T, \sigma_{30}^T, \sigma_{40}^T]^T$ are set to be
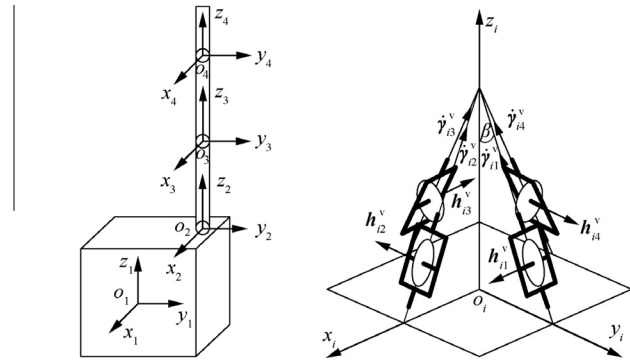
$$\begin{cases} R_0 = [0.2, \quad -0.3, \quad 0.3]^T \text{ m} \\ \sigma_{10} = [0.0109, \quad -0.0189, \quad 0.0378]^T \\ \sigma_{20} = [0.2679, \quad 0, \quad 0]^T \\ \sigma_{30} = [-0.2679, \quad 0, \quad 0]^T \\ \sigma_{40} = [0.2588, \quad 0.0694, \quad 0]^T \end{cases}$$

### 7.2. Control objective

The control objective is to drive the manipulator variable $\Psi = [R^T, \sigma_1^T, R_4^T, \sigma_4^T]^T$ to track its desired trajectory $\Psi_d(t) = [R_d^T(t), \sigma_{1d}^T(t), R_{4d}^T(t), \sigma_{4d}^T(t)]^T$. Here the endpoint of the link $B_4$ is taken as the reference point of the end effector/payload position $R_4$, and then $R_4$ can be expressed as

$$R_4 = R + A_{0,1}r_{1,2} + A_{0,2}r_{2,3} + A_{0,3}r_{3,4} + A_{0,4}r_{4t} \quad (63)$$

where $r_{4t} = [0, 0, 0.6]^T$ m is the endpoint position of the link $B_4$ in $F_4$. Because $R$ is not controlled, we then use the current $R$, $\dot{R}$ and $\ddot{R}$ as the desired values of $R_d(t)$, $\dot{R}_d(t)$ and $\ddot{R}_d(t)$, respectively. The initial values of $\sigma_{1d}(t)$, $R_{4d}(t)$ and $\sigma_{4d}(t)$ are determined by the initial values of the desired system displacements in $q_{d0} = [R_{d0}^T, \sigma_{1d0}^T, \sigma_{2d0}^T, \sigma_{3d0}^T, \sigma_{4d0}^T]^T$ which are set to be

**Table 1**    System inertial parameters.

| Body number | Mass (kg) | | First moment (true) (kg · m) | Moment of inertia (kg · m²) | |
|---|---|---|---|---|---|
| | True | Nominal | | True | Nominal |
| $B_1$ | 3000 | 2400 | $[0, 15, 0]^T$ | $\begin{bmatrix} 1500 & -37 & -26.5 \\ -37 & 1800 & -15 \\ -26.5 & -15 & 2000 \end{bmatrix}$ | $\begin{bmatrix} 1200 & -29.6 & -21.2 \\ -29.6 & 1440 & -12 \\ -21.2 & -12 & 1600 \end{bmatrix}$ |
| $B_2$ | 60 | 90 | $[0, 0, 45]^T$ | diag $(45, 45, 5.5)$ | diag $(67.5, 67.5, 8.25)$ |
| $B_3$ | 60 | 42 | $[0, 0, 45]^T$ | diag $(45, 45, 5.5)$ | diag $(31.5, 31.5, 3.85)$ |
| $B_4$ | 300 | 150 | $[0, 0, 90]^T$ | diag $(36, 36, 7.5)$ | diag $(18, 18, 3.75)$ |

$$\begin{cases} \boldsymbol{R}_{d0} = [0.2, -0.3, 0.3]^{\mathrm{T}} \text{ m} \\ \boldsymbol{\sigma}_{1d0} = [0.0164, \quad -0.0284, \quad 0.0568]^{\mathrm{T}} \\ \boldsymbol{\sigma}_{2d0} = [0.1989, \quad 0, \quad 0]^{\mathrm{T}} \\ \boldsymbol{\sigma}_{3d0} = [-0.3395, \quad 0, \quad 0]^{\mathrm{T}} \\ \boldsymbol{\sigma}_{4d0} = [0.1921, \quad 0.0515, \quad 0]^{\mathrm{T}} \end{cases}$$

By Eq. (63), the corresponding initial values of $\boldsymbol{\sigma}_{1d}(t)$, $\boldsymbol{R}_{4d}(t)$ and $\boldsymbol{\sigma}_{4d}(t)$ are then computed as

$$\begin{cases} \boldsymbol{\sigma}_{1d0} = [0.0164, \quad -0.0284, \quad 0.0568]^{\mathrm{T}} \\ \boldsymbol{R}_{4d0} = [0.0604, \quad 0.3495, \quad 2.9557]^{\mathrm{T}} \text{ m} \\ \boldsymbol{\sigma}_{4d0} = [0.1921, \quad 0.0515, \quad 0]^{\mathrm{T}} \end{cases}$$

$\boldsymbol{\sigma}_{1d}(t)$ and $\boldsymbol{\sigma}_{4d}(t)$ are determined by quintic polynomials with the desired initial values of $\boldsymbol{\sigma}_{1d0}$ and $\boldsymbol{\sigma}_{4d0}$ and the desired final values of $\boldsymbol{\sigma}_{1df} = [0, \quad 0, \quad 0]^{\mathrm{T}}$ and $\boldsymbol{\sigma}_{4df} = [0, \quad 0, \quad 0]^{\mathrm{T}}$, and given as

$$\boldsymbol{\sigma}_{id}(t) = \begin{cases} \boldsymbol{\Phi}_{\sigma_i} \boldsymbol{T} + \boldsymbol{\sigma}_{id0} & t_0 \leqslant t \leqslant t_{\mathrm{f}} \\ \boldsymbol{\sigma}_{idf} & t > t_{\mathrm{f}} \end{cases}, \quad i = 1, 4$$

where $t_0 = 0$ s, $t_{\mathrm{f}} = 30$ s, $\boldsymbol{T} = \begin{bmatrix} t^5, & t^4, & t^3 \end{bmatrix}^{\mathrm{T}}$, and

$$\begin{cases} \boldsymbol{\Phi}_{\sigma_1} = \begin{bmatrix} -4.0459 \times 10^{-9} & 3.0344 \times 10^{-7} & 6.0688 \times 10^{-6} \\ 7.0077 \times 10^{-9} & -5.2558 \times 10^{-7} & 1.0512 \times 10^{-5} \\ -1.4015 \times 10^{-8} & 1.0512 \times 10^{-6} & -2.1023 \times 10^{-5} \end{bmatrix} \\ \boldsymbol{\Phi}_{\sigma_4} = \begin{bmatrix} -4.7441 \times 10^{-8} & 3.5580 \times 10^{-6} & -7.1161 \times 10^{-5} \\ -1.2712 \times 10^{-8} & 9.5338 \times 10^{-7} & -1.9068 \times 10^{-5} \\ 0 & 0 & 0 \end{bmatrix} \end{cases}$$

It is easy to verify that $\boldsymbol{\sigma}_{id}(t) \, (i = 1, 4)$ satisfies the following constraints:

$$\begin{cases} \boldsymbol{\sigma}_{id}(t_0) = \boldsymbol{\sigma}_{id0}, \quad \boldsymbol{\sigma}_{id}(t_{\mathrm{f}}) = \boldsymbol{\sigma}_{idf} \\ \dot{\boldsymbol{\sigma}}_{id}(t_0) = \ddot{\boldsymbol{\sigma}}_{id}(t_0) = \boldsymbol{0} \\ \dot{\boldsymbol{\sigma}}_{id}(t_{\mathrm{f}}) = \ddot{\boldsymbol{\sigma}}_{id}(t_{\mathrm{f}}) = \boldsymbol{0} \end{cases}$$

Because $\boldsymbol{\sigma}_{1df}$ and $\boldsymbol{\sigma}_{4df}$ are constant values of zero, the attitudes of both the base and the end effector/payload are supposed to maintain stable control along desired approaching trajectories.

When $t_0 \leqslant t \leqslant t_{\mathrm{f}}$, $\boldsymbol{R}_{4d}(t)$ is also determined by quintic polynomials with the desired initial values of $\boldsymbol{R}_{4d0}$ and the desired value of $\boldsymbol{R}_{4d}(t)$ at $t = t_{\mathrm{f}}$, $\boldsymbol{R}_{4d}(t_{\mathrm{f}}) =$
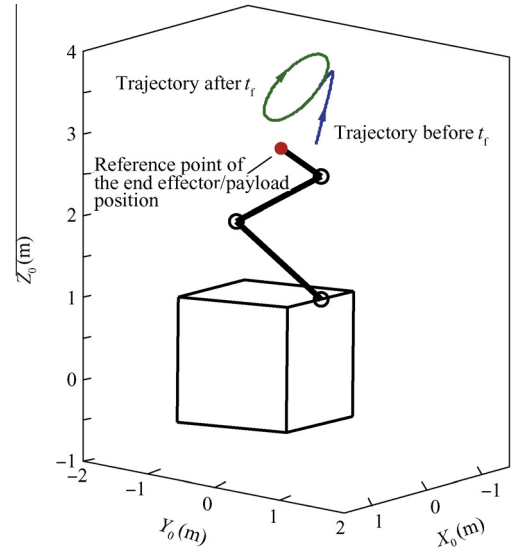


**Fig. 4** System initial configuration and desired position trajectory of end effector/payload.

where

$$\begin{cases} \boldsymbol{\Phi}_R = \begin{bmatrix} -6.9423 \times 10^{-8} & 7.4473 \times 10^{-6} & -1.7921 \times 10^{-4} \\ 6.5902 \times 10^{-8} & -3.4562 \times 10^{-6} & 2.6797 \times 10^{-5} \\ 4.2272 \times 10^{-7} & -2.9129 \times 10^{-5} & 5.0927 \times 10^{-4} \end{bmatrix} \\ \boldsymbol{R}_{4df}(t) = \begin{bmatrix} r\cos(\omega_{\mathrm{c}}t + \theta_1) + X_0 \\ r\sin(\omega_{\mathrm{c}}t + \theta_1)\cos\theta_2 + Y_0 \\ r\sin(\omega_{\mathrm{c}}t + \theta_1)\sin\theta_2 + Z_0 \end{bmatrix} \end{cases}$$

Therein, $r = 0.5$ m, $\omega_{\mathrm{c}} = \pi/20$, $\theta_1 = -\pi/3$, $\theta_2 = \pi/3$, $X_0 = Y_0 = 0$ m and $Z_0 = 3.6$ m. $\boldsymbol{R}_{4df}(t)$ is actually a periodic circle trajectory in inertial space, and $\boldsymbol{\Phi}_R \boldsymbol{T} + \boldsymbol{R}_{4d}(t_{\mathrm{f}})$ is a smooth trajectory from $\boldsymbol{R}_{4d0}$ to $\boldsymbol{R}_{4df}(t)$ which intersects $\boldsymbol{R}_{4df}(t)$ at the point of $\boldsymbol{R}_{4d}(t_{\mathrm{f}})$. The parameters ensure that $\boldsymbol{R}_{4d}(t)$ is doubly differentiable. Fig. 4 shows the system initial configuration and the desired position trajectory of the end effector/payload.

The Jacobian matrix $\boldsymbol{J}(\boldsymbol{q})$ which associates the manipulator variable $\boldsymbol{\Psi}$ with system displacement $\boldsymbol{q}$ is

$$\boldsymbol{J}(\boldsymbol{q}) = \begin{bmatrix} \boldsymbol{I} & \boldsymbol{0}_{3\times3} & \boldsymbol{0}_{3\times3} & \boldsymbol{0}_{3\times3} & \boldsymbol{0}_{3\times3} \\ \boldsymbol{0}_{3\times3} & \boldsymbol{I} & \boldsymbol{0}_{3\times3} & \boldsymbol{0}_{3\times3} & \boldsymbol{0}_{3\times3} \\ \boldsymbol{I} & -\boldsymbol{A}_{0,1}\boldsymbol{r}_{1,2}^{\times}\boldsymbol{H}_1^{-1}(\boldsymbol{\sigma}_1) & -\boldsymbol{A}_{0,2}\boldsymbol{r}_{2,3}^{\times}\boldsymbol{H}_2^{-1}(\boldsymbol{\sigma}_2) & -\boldsymbol{A}_{0,3}\boldsymbol{r}_{3,4}^{\times}\boldsymbol{H}_3^{-1}(\boldsymbol{\sigma}_3) & -\boldsymbol{A}_{0,4}\boldsymbol{r}_{4t}^{\times}\boldsymbol{H}_4^{-1}(\boldsymbol{\sigma}_4) \\ \boldsymbol{0}_{3\times3} & \boldsymbol{0}_{3\times3} & \boldsymbol{0}_{3\times3} & \boldsymbol{0}_{3\times3} & \boldsymbol{I} \end{bmatrix}$$

$[-0.4330, \quad -0.1250, \quad 3.3835]^{\mathrm{T}}$ m. When $t > t_{\mathrm{f}}$, $\boldsymbol{R}_{4d}(t)$ is a predesigned continuous trajectory instead of a constant. The expression of $\boldsymbol{R}_{4d}(t)$ is given as

$$\boldsymbol{R}_{4d}(t) = \begin{cases} \boldsymbol{\Phi}_R \boldsymbol{T} + \boldsymbol{R}_{4d}(t_{\mathrm{f}}) & t_0 \leqslant t \leqslant t_{\mathrm{f}} \\ \boldsymbol{R}_{4df}(t) & t > t_{\mathrm{f}} \end{cases}$$

Based on $\boldsymbol{\Psi}_d(t)$ given above, the desired displacement $\boldsymbol{q}_d$, as well as its first and second time derivatives $\dot{\boldsymbol{q}}_d$ and $\ddot{\boldsymbol{q}}_d$, can be obtained using the trajectory planning algorithm presented in Section 4 and the Jacobian matrix $\boldsymbol{J}(\boldsymbol{q})$ given above, and then the control objective is to drive $\boldsymbol{\sigma}_i \, (i = 1, 2, 3, 4)$ to track the desired trajectory $\boldsymbol{\sigma}_{id}$ in $\boldsymbol{q}_d$.

**Table 2** System control parameters.

| Controller | $N$ | $q_0$ | $q_1$ | $q_2$ | $q_3$ | $\psi_0$ | $\psi_1$ | $\psi_2$ | $\psi_3$ | $a$ | $b$ | $\delta$ | $\varepsilon$ | $C$ | $K_D$ |
|---|---|---|---|---|---|---|---|---|---|---|---|---|---|---|---|
| $B_1$ | 3 | 5 | 5 | 5 | 5 | 0.010 | 0.010 | 0.010 | 0.010 | 0.004 | 3750 | 0.004 | 0.02 | $[0.3I, I]$ | $0.3I$ |
| $B_2$ | 3 | 5 | 5 | 5 | 5 | 0.005 | 0.005 | 0.005 | 0.005 | 0.010 | 1500 | 0.010 | 0.01 | $[0.5I, I]$ | $0.5I$ |
| $B_3$ | 3 | 5 | 5 | 5 | 5 | 0.005 | 0.005 | 0.005 | 0.005 | 0.010 | 1500 | 0.010 | 0.01 | $[0.5I, I]$ | $0.5I$ |
| $B_4$ | 3 | 5 | 5 | 5 | 5 | 0.005 | 0.005 | 0.005 | 0.005 | 0.010 | 1500 | 0.010 | 0.01 | $[0.5I, I]$ | $0.5I$ |
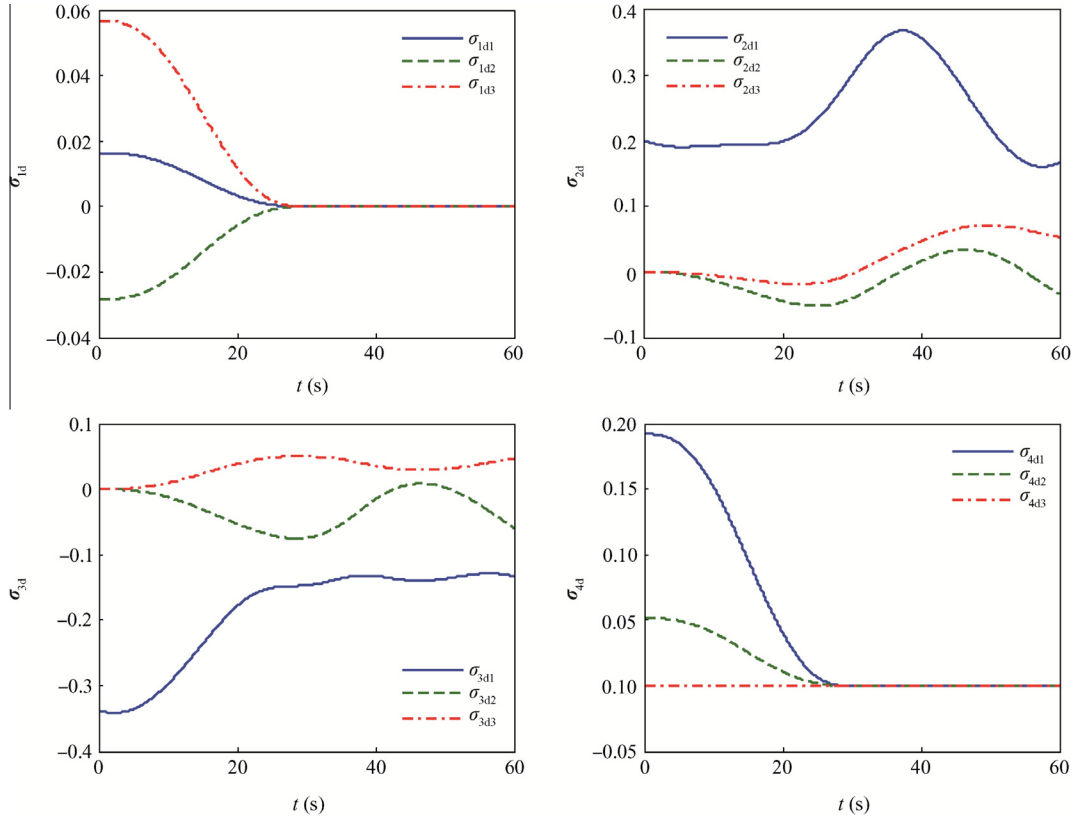


**Fig. 5** Desired trajectories of $\boldsymbol{\sigma}_i\,(i = 1, 2, 3, 4)$.

### 7.3. Disturbance torques

The disturbance torques taken into consideration mainly include two parts: the joint friction torques and other possible disturbance torques. Precise modeling of the friction torque of a ball joint is quite complex, and in the simulation, the following model is used to roughly simulate the friction torque of joint $i$ acting on $B_i\,(i = 2, 3, 4)$.

$$\boldsymbol{T}_{hi} = -\lambda_{ci}\mathbf{sat}(\boldsymbol{\omega}_i - \boldsymbol{A}_{i,i-1}\boldsymbol{\omega}_{i-1}, \boldsymbol{\varsigma}_i) - \lambda_{ti}(\boldsymbol{\omega}_i - \boldsymbol{A}_{i,i-1}\boldsymbol{\omega}_{i-1}),$$
$$i = 2, 3, 4$$

where, for any $\boldsymbol{x} = [x_1,\ x_2,\ x_3]^T \in \mathbf{R}^3$ and $\boldsymbol{\varsigma} = [\varsigma_1,\ \varsigma_2,\ \varsigma_3]^T \in \mathbf{R}^3$, $\mathbf{sat}(\boldsymbol{x}, \boldsymbol{\varsigma}) = [\mathrm{sat}(x_1, \varsigma_1),\ \mathrm{sat}(x_2, \varsigma_2),\ \mathrm{sat}(x_3, \varsigma_3)]^T$, and therein, $\mathrm{sat}(x_j, \varsigma_j)\,(j = 1, 2, 3)$ is a saturation function defined as

$$\mathrm{sat}(x_j, \varsigma_j) = \begin{cases} \mathrm{sign}(x_j) & |x_j| \geqslant \varsigma_j \\ x_j/\varsigma_j & |x_j| < \varsigma_j \end{cases}, \quad j = 1, 2, 3$$

Other possible disturbance torques acting on $B_i$ $(i = 1, 2, 3, 4)$ are considered to be the sum of a constant torque and a periodic torque with the argument of time $t$, and given as

$$\boldsymbol{T}_{pi} = \boldsymbol{T}_{pi0} + \boldsymbol{T}_{pip}\sin(\omega_{pi}t) \quad i = 1, 2, 3, 4$$

Note that when the friction torque of joint $i$ acts on $B_i$, its reaction torque will also act on $B_{i-1}$, and then the disturbance torques in $\boldsymbol{F}_d$ (see Eq. (26)) in the simulation are given as

$$\begin{cases} \boldsymbol{T}_{d1} = \boldsymbol{T}_{p1} - \boldsymbol{A}_{1,2}\boldsymbol{T}_{h2} \\ \boldsymbol{T}_{d2} = \boldsymbol{T}_{p2} + \boldsymbol{T}_{h2} - \boldsymbol{A}_{2,3}\boldsymbol{T}_{h3} \\ \boldsymbol{T}_{d3} = \boldsymbol{T}_{p3} + \boldsymbol{T}_{h3} - \boldsymbol{A}_{3,4}\boldsymbol{T}_{h4} \\ \boldsymbol{T}_{d4} = \boldsymbol{T}_{p4} + \boldsymbol{T}_{h4} \end{cases}$$

The related constant parameters are chosen to be

$$\begin{cases} \lambda_{c2} = 0.15\,\mathrm{N \cdot m}, & \lambda_{c3} = \lambda_{c4} = 0.1\mathrm{N \cdot m} \\ \lambda_{t2} = 0.07\,\mathrm{N \cdot m \cdot s/rad} \\ \lambda_{t3} = \lambda_{t4} = 0.05\,\mathrm{N \cdot m \cdot s/rad} \\ \boldsymbol{\zeta}_2 = \boldsymbol{\zeta}_3 = \boldsymbol{\zeta}_4 = [2,\quad 2,\quad 2]^T \times 10^{-3}\,\mathrm{rad/s} \end{cases},$$
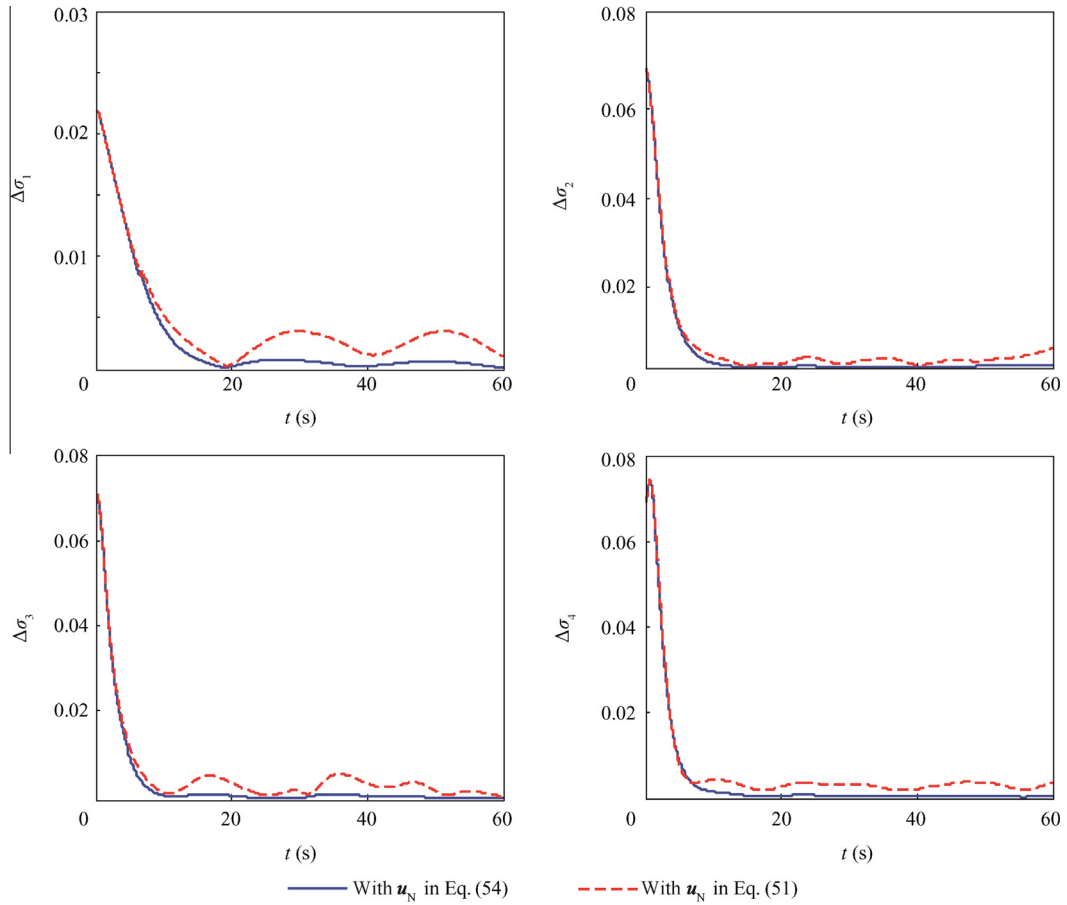
**Fig. 6** Control errors of $\boldsymbol{\sigma}_i\,(i = 1, 2, 3, 4)$.
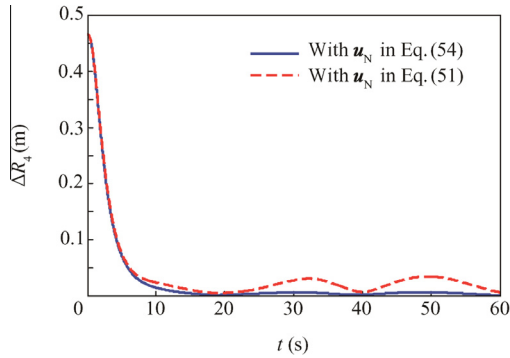


**Fig. 7** Position errors of the end effector/payload.

$$
\begin{cases}
\boldsymbol{T}_{\mathrm{p}10} = [0.15, \quad 0.15, \quad 0.15]^{\mathrm{T}} \, \mathrm{N} \cdot \mathrm{m} \\
\boldsymbol{T}_{\mathrm{p}20} = [0.1, \quad 0.1, \quad 0.1]^{\mathrm{T}} \, \mathrm{N} \cdot \mathrm{m} \\
\boldsymbol{T}_{\mathrm{p}30} = \boldsymbol{T}_{\mathrm{p}40} = [0.08, \quad 0.08, \quad 0.08]^{\mathrm{T}} \, \mathrm{N} \cdot \mathrm{m} \\
\boldsymbol{T}_{\mathrm{p}1\mathrm{p}} = [0.15, \quad -0.2, \quad -0.15]^{\mathrm{T}} \, \mathrm{N} \cdot \mathrm{m} \\
\boldsymbol{T}_{\mathrm{p}2\mathrm{p}} = [0.1, \quad -0.15, \quad -0.1]^{\mathrm{T}} \, \mathrm{N} \cdot \mathrm{m} \\
\boldsymbol{T}_{\mathrm{p}3\mathrm{p}} = \boldsymbol{T}_{\mathrm{p}4\mathrm{p}} = [0.08, \quad -0.12, \quad -0.08]^{\mathrm{T}} \, \mathrm{N} \cdot \mathrm{m}
\end{cases},
$$

$$
\omega_{\mathrm{p}1} = 0.3 \, \mathrm{rad/s}, \quad \omega_{\mathrm{p}2} = \omega_{\mathrm{p}3} = \omega_{\mathrm{p}4} = 0.5 \, \mathrm{rad/s}
$$

### 7.4. Control parameters

For the controller of $B_i\ (i = 1, 2, 3, 4)$, the function $P(x)$ in Eq. (55) is denoted as $P_i(x)$ and designed as

$$
P_i(x) = \begin{cases} a_i \tanh(b_i x) & x \leqslant \delta_i \\ x & x > \delta_i \end{cases}, \quad i = 1, 2, 3, 4
$$

where the parameters of $a_i$, $b_i$ and $\delta_i$ which guarantee Condition 1, as well as other control parameters, are listed together in Table 2.

For each cluster of CMGs, the null motion coefficient is chosen to be the same value of $\alpha_i = 0.5\,(i = 1, 2, 3, 4)$.

### 7.5. Simulation results and analysis

Fig. 5 shows the desired trajectories of $\boldsymbol{\sigma}_i\,(i = 1, 2, 3, 4)$, $\boldsymbol{\sigma}_{id} = [\,\sigma_{id1}, \quad \sigma_{id2}, \quad \sigma_{id3}\,]^{\mathrm{T}}$, solved using the trajectory planning algorithm presented in Section 4 based on the given desired manipulator variable $\boldsymbol{\Psi}_{\mathrm{d}}(t)$. Fig. 6 shows the control errors of $\boldsymbol{\sigma}_i\ (i = 1, 2, 3, 4)$ defined as $\Delta\sigma_i = ||\boldsymbol{\sigma}_i - \boldsymbol{\sigma}_{id}||$, and Fig. 7 shows the position errors of the end effector/payload defined as $\Delta R_4 = ||\boldsymbol{R}_4 - \boldsymbol{R}_{4\mathrm{d}}(t)||$ under the direct control of $\boldsymbol{\sigma}_i$. For comparison, the results using the control law Eq. (45) with $\boldsymbol{u}_{\mathrm{N}}$ given in Eq. (54) (the proposed control law in this paper) and those using the control law Eq. (45) with $\boldsymbol{u}_{\mathrm{N}}$ given in Eq. (51) are both presented in Figs. 6 and 7. The two control laws use the same control parameters (if they have) as given in
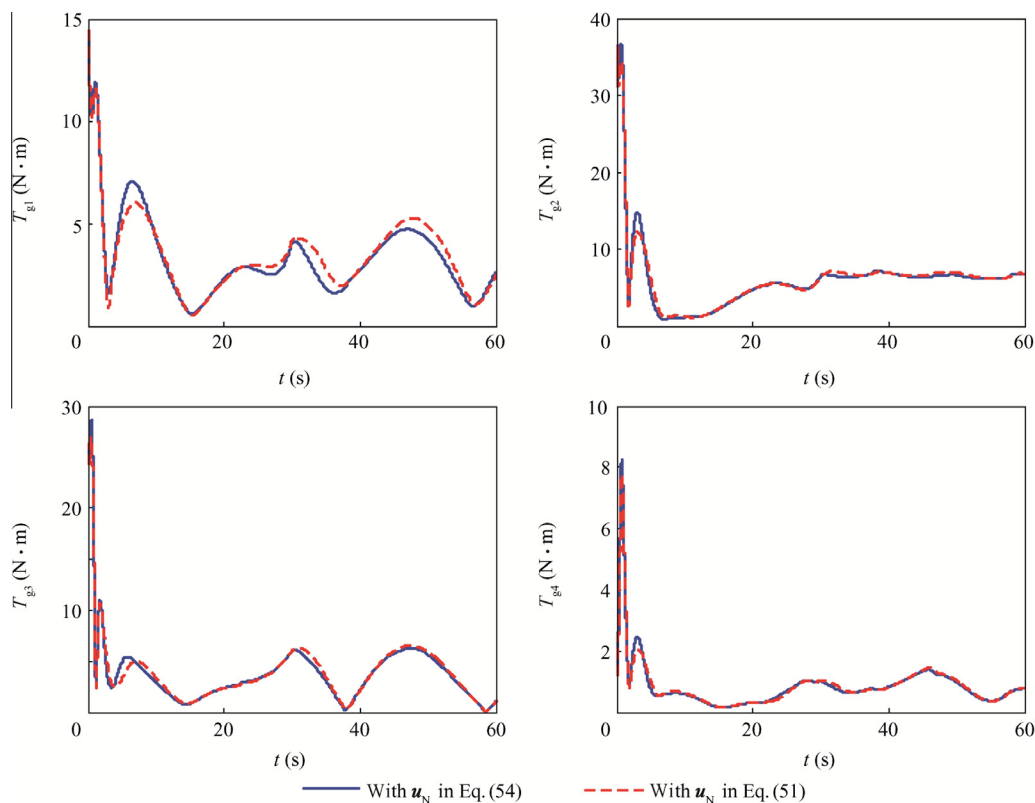
**Fig. 8** Magnitudes of $T_{gi}$ $(i = 1, 2, 3, 4)$.

Section 7.4 to obtain comparable results. As can be seen, the control errors of the control law with $u_N$ given in Eq. (54) are conspicuously smaller than those of the control law with $u_N$ given in Eq. (51), which verifies the effectiveness of the proposed improvements in the control law and adaptation laws.

Fig. 8 gives the magnitudes of $T_{gi}$, i.e., $T_{gi} = ||T_{gi}||$ $(i = 1, 2, 3, 4)$. By comparing $T_{gi}$ produced by $u_N$ given in Eq. (54) with those produced by $u_N$ given in Eq. (51), we can see that, as expected, the control law with $u_N$ given in Eq. (54) does not produce noticeably larger control torque than that with $u_N$ given in Eq. (51) although it does achieve better control accuracy. Moreover, no chattering phenomenon occurs in the simulations of both two controllers due to their continuity in control inputs. Further simulation results show that if the amplification range in the adaptation laws is extended, better control accuracy may be achieved but at the possible cost of increasing the magnitude of the control torques.

The steering law with null motion for the CMGs works well during the simulation. Fig. 9 shows the configuration singularity measurements of the CMGs (the results in Fig. 9 are achieved by the control law with $u_N$ given in Eq. (54)), including those with null motion and without null motion. Though the CMG clusters do not run into singularity even when the null motion is not added, in most of the time, the measurements with null motion are much larger than those without null motion, which indicates effective singularity avoidance of the null motion.

Fig. 10 shows system configurations at different moments during the control. The coordinate with solid line axes represents $F_4$, and that with dotted line axes represents the desired orientation of $F_4$. The same color represents the same axis. The origin of $F_4$ is located at the position reference point of the end effector/payload, and that of the desired coordinate is located at the desired position of the end effector/payload. At the initial moment, both the position and the orientation of the end effector/payload have conspicuous deviations from the desired ones, and the base attitude also has visible deviation from the desired attitude of $[0, 0, 0]^T$. Under the control of the proposed control law, the deviations decrease gradually and enter into a small boundary ultimately.

## 8. Conclusions

(1) Decentralized controller design for trajectory tracking of the space robot system faces the challenge of large system uncertainty with unknown upper bound. The sliding mode controller with the improved adaptation laws proposed in this paper can achieve uniformly ultimate boundedness of the closed loop system. The amplification function introduced in the adaptation laws effectively reduces the control error without notably increasing the control input magnitude provided that the amplification range is properly selected, and the control law is free from the chattering problem due to its continuity. The proposed controller is expected to be applicable to systems with different configurations because the controller for each link is designed separately as a sole system.

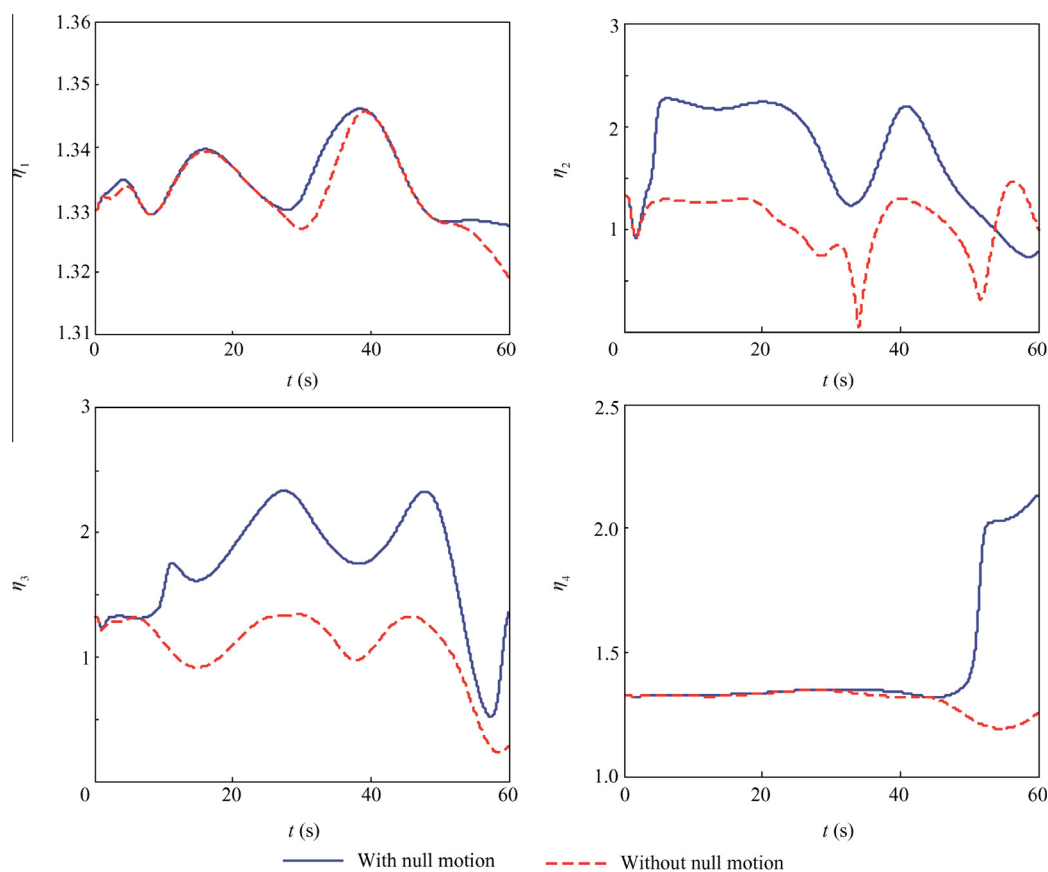(2) It should also be noticed that as angular momentum devices, the CMGs always face the risk of angular

Fig. 9    Singularity measurements of CMGs.



(a) $t = 0$ s
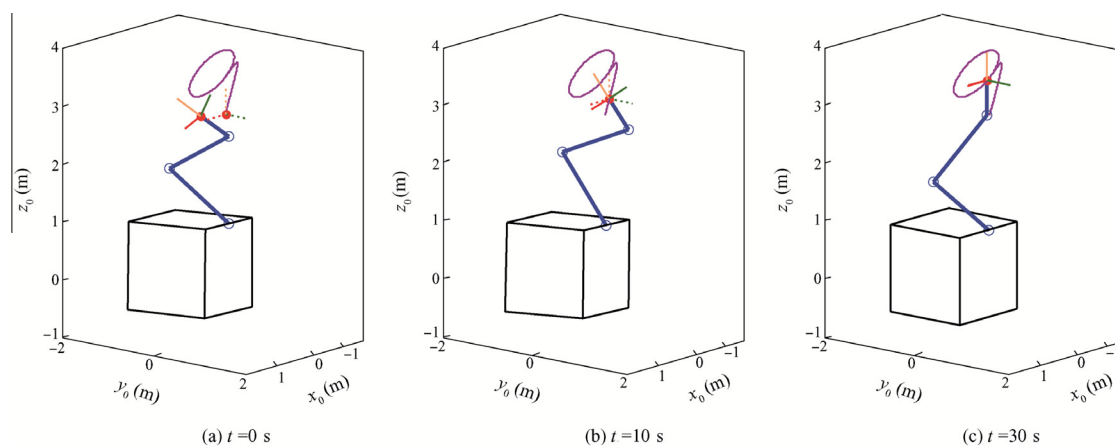
(b) $t = 10$ s

(c) $t = 30$ s

Fig. 10    System configuration at different moments during control.

momentum saturation. Therefore, the CMG-actuating design cannot be applied to terrestrial robotic systems due to continuous gravitational torques. Even in space environment, reducing the possibility of saturation is still of great significance; therefore the approach to realize this objective is regarded as important future work. The approach may be implemented along two different routes. From the angle of hardware, we can increase the CMG angular momentum by increasing either the

moment of inertia or the spin rate of the CMG rotor to reduce the possibility of saturation; however, such methods will definitely increase the mass of the CMGs, which, to some extent, equates to increasing the payload mass of the robotic manipulator. Therefore, we need an appropriate optimization method to balance the angular moment of the CMGs and the load capacity of the robotic manipulator. From the angle of algorithm, we may utilize the redundancy of DOC of the joints to

redistribute the three-axis angular momentum of each link so as to avoid saturation. In other words, with the redundancy of DOC of the joints, we may seek a trajectory helping saturation avoidance in joint space from infinite trajectories which satisfy the end effector/payload trajectory constraints.

## Acknowledgement

## Appendix A

$$M(q) = \begin{bmatrix} mI & -A_{0,1}(s_1^*)^\times & -A_{0,2}(s_2^*)^\times & -A_{0,3}(s_3^*)^\times & -A_{0,4}(s_4^*)^\times & \cdots & -A_{0,n}(s_n^*)^\times \\ * & I_1^* & -r_{1,2}^\times A_{1,2}(s_2^*)^\times & -r_{1,2}^\times A_{1,3}(s_3^*)^\times & -r_{1,2}^\times A_{1,4}(s_4^*)^\times & \cdots & -r_{1,2}^\times A_{1,n}(s_n^*)^\times \\ * & * & I_2^* & -r_{2,3}^\times A_{2,3}(s_3^*)^\times & -r_{2,3}^\times A_{2,4}(s_4^*)^\times & \cdots & -r_{2,3}^\times A_{2,n}(s_n^*)^\times \\ * & * & * & I_3^* & -r_{3,4}^\times A_{3,4}(s_4^*)^\times & \cdots & -r_{3,4}^\times A_{3,n}(s_n^*)^\times \\ * & * & * & * & I_4^* & \cdots & -r_{4,5}^\times A_{4,n}(s_n^*)^\times \\ * & * & * & * & * & & * \\ * & * & * & * & * & * & I_n^* \end{bmatrix} \tag{A1}$$

where $m$ is the total mass of the system, and

$$\begin{cases} s_i^* = s_i + \sum_{j=i+1}^{n} m_j r_{i,i+1} \\ I_i^* = I_i' + \sum_{j=i+1}^{n} m_j (r_{i,i+1}^\times)^\mathrm{T} r_{i,i+1}^\times \end{cases}$$

Therein, $m_j$ is the mass of $B_j$, $s_i = \int_{B_i} r_i \mathrm{d}m$ is the first moment of $B_i$ in $F_i$, and $I_i' = \int_{B_i} (r_i^\times)^\mathrm{T} r_i^\times \mathrm{d}m$ is the moment of inertia of $B_i$ in $F_i$.

$$Q(q, v) = \begin{bmatrix} Q_0^\mathrm{T}(q, v), & Q_1^\mathrm{T}(q, v), & \ldots, & Q_n^\mathrm{T}(q, v) \end{bmatrix}^\mathrm{T} \tag{A2}$$

where

$$\begin{cases} Q_0(q, v) = -\sum_{j=1}^{n} A_{0,j} \omega_j^\times (s_j^*)^\times \omega_j \\ Q_1(q, v) = \omega_1^\times I_1^* \omega_1 - r_{1,2}^\times \sum_{j=2}^{n} A_{1,j} \omega_j^\times (s_j^*)^\times \omega_j \\ Q_i(q, v) = -\sum_{j=1}^{i-1} (s_i^*)^\times A_{i,j} \omega_j^\times r_{j,j+1}^\times \omega_j + \omega_i^\times I_i^* \omega_i \\ \qquad\qquad -r_{i,i+1}^\times \sum_{j=i+1}^{n} A_{i,j} \omega_j^\times (s_j^*)^\times \omega_j \\ i = 2, 3, \ldots, n \end{cases}$$

## Appendix B

Define a Lyapunov function as

$$V = \frac{1}{2} S^\mathrm{T} S + \frac{1}{2} q_0^{-1} \tilde{c}_0^2 + \frac{1}{2} q_1^{-1} \tilde{c}_1^2 + \ldots + \frac{1}{2} q_N^{-1} \tilde{c}_N^2 \tag{B1}$$

where

$$\tilde{c}_0 = \bar{c}_0 - c_0, \quad \tilde{c}_1 = \bar{c}_1 - c_1, \ldots, \tilde{c}_N = \bar{c}_N - c_N$$

Differentiating $V$ with respect to time yields

$$\dot{V} = S^\mathrm{T} \dot{S} + \sum_{k=0}^{N} q_k^{-1} \tilde{c}_k \dot{\tilde{c}}_k \tag{B2}$$

If $\bar{\rho} \| B^T C^T S \|^2 > \varepsilon P(\| B^\mathrm{T} C^\mathrm{T} S \|)$, Eq. (B2) becomes

$$\begin{aligned} \dot{V} &= S^\mathrm{T}(-K_\mathrm{D} S + CB u_\mathrm{N} + CB d) + \sum_{k=0}^{N} q_k^{-1} c_k \dot{c}_k \\ &= -S^\mathrm{T} K_\mathrm{D} S - P(\| B^\mathrm{T} C^\mathrm{T} S \|)(\bar{c}_0 + \bar{c}_1 \| x \| + \ldots + \bar{c}_n \| x \|^N) \\ &\quad + S^\mathrm{T} CB d + \sum_{k=0}^{N} q_k^{-1} c_k \dot{c}_k \leqslant -S^\mathrm{T} K_\mathrm{D} S \\ &\quad - P(\| B^\mathrm{T} C^\mathrm{T} S \|)(\bar{c}_0 + \bar{c}_1 \| x \| + \ldots + \bar{c}_N \| x \|^N) \\ &\quad + P(\| B^\mathrm{T} C^\mathrm{T} S \|)(c_0 + c_1 \| x \| + \ldots + c_N \| x \|^N) + \sum_{k=0}^{N} q_k^{-1} c_k \dot{c}_k \\ &= -S^\mathrm{T} K_\mathrm{D} S - c_0 P(\| B^\mathrm{T} C^\mathrm{T} S \|) - c_1 P(\| B^\mathrm{T} C^\mathrm{T} S \|) \| x \| - \ldots \\ &\quad - \tilde{c}_N P(\| B^\mathrm{T} C^\mathrm{T} S \|) \| x \|^N + \sum_{k=0}^{N} q_k^{-1} c_k \dot{c}_k \\ &= -S^\mathrm{T} K_\mathrm{D} S - c_0 P(\| B^\mathrm{T} C^\mathrm{T} S \|) - \tilde{c}_1 P(\| B^\mathrm{T} C^\mathrm{T} S \|) \| x \| - \ldots \\ &\quad - \tilde{c}_N P(\| B^\mathrm{T} C^\mathrm{T} S \|) \| x \|^N + \tilde{c}_0 [-\psi_0 \bar{c}_0 + P(\| B^\mathrm{T} C^\mathrm{T} S \|)] \\ &\quad + \tilde{c}_1 [-\psi_1 \bar{c}_1 + P(\| B^\mathrm{T} C^\mathrm{T} S \|) \| x \|] + \ldots \\ &\quad + \tilde{c}_N [-\psi_N \bar{c}_N + P(\| B^\mathrm{T} C^\mathrm{T} S \|) \| x \|^N] \\ &= -S^\mathrm{T} K_\mathrm{D} S - \psi_0 c_0 \bar{c}_0 - \psi_1 c_1 \bar{c}_1 - \ldots - \psi_N c_N \bar{c}_N \\ &= -S^\mathrm{T} K_\mathrm{D} S - \psi_0 \left(\frac{1}{2} c_0 - \bar{c}_0\right)^2 - \psi_1 \left(\frac{1}{2} c_1 - \bar{c}_1\right)^2 - \ldots \\ &\quad - \psi_N \left(\frac{1}{2} c_N - \bar{c}_N\right)^2 + \frac{1}{4} \psi_0 c_0^2 + \frac{1}{4} \psi_1 c_1^2 + \ldots + \frac{1}{4} \psi_N c_N^2 \\ &= -S^\mathrm{T} K_\mathrm{D} S - \psi_0 \left(\frac{1}{2} c_0 - \bar{c}_0\right)^2 - \psi_1 \left(\frac{1}{2} c_1 - \bar{c}_1\right)^2 - \ldots \\ &\quad - \psi_N \left(\frac{1}{2} c_N - \bar{c}_N\right)^2 + \kappa_1 \end{aligned} \tag{B3}$$

where $\kappa_1 = \sum_{k=0}^{N} \frac{1}{4} \psi_i c_i^2$ is a constant.

If $\bar{\rho}\|\boldsymbol{B}^{\mathrm{T}}\boldsymbol{C}^{\mathrm{T}}\boldsymbol{S}\|^2 \leqslant \varepsilon P(\|\boldsymbol{B}^{\mathrm{T}}\boldsymbol{C}^{\mathrm{T}}\boldsymbol{S}\|)$, Eq. (B2) can be written as

$$\dot{V} = \boldsymbol{S}^{\mathrm{T}}(-\boldsymbol{K}_{\mathrm{D}}\boldsymbol{S} + \boldsymbol{C}\boldsymbol{B}\boldsymbol{u}_{\mathrm{N}} + \boldsymbol{C}\boldsymbol{B}\boldsymbol{d}) + \sum_{k=0}^{N} q_k^{-1} c_k \dot{c}_k$$

$$= -\boldsymbol{S}^{\mathrm{T}}\boldsymbol{K}_{\mathrm{D}}\boldsymbol{S} - \frac{\|\boldsymbol{B}^{\mathrm{T}}\boldsymbol{C}^{\mathrm{T}}\boldsymbol{S}\|^2}{\varepsilon}\bar{\rho}^2 + \boldsymbol{S}^{\mathrm{T}}\boldsymbol{C}\boldsymbol{B}\boldsymbol{d} + \sum_{k=0}^{N} q_k^{-1} c_k \dot{c}_k$$

$$\leqslant -\boldsymbol{S}^{\mathrm{T}}\boldsymbol{K}_{\mathrm{D}}\boldsymbol{S} - \frac{\|\boldsymbol{B}^{\mathrm{T}}\boldsymbol{C}^{\mathrm{T}}\boldsymbol{S}\|^2}{\varepsilon}\bar{\rho}^2 + P(\|\boldsymbol{B}^{\mathrm{T}}\boldsymbol{C}^{\mathrm{T}}\boldsymbol{S}\|)\rho + \sum_{k=0}^{N} q_k^{-1} c_k \dot{c}_k$$

$$= -\boldsymbol{S}^{\mathrm{T}}\boldsymbol{K}_{\mathrm{D}}\boldsymbol{S} - \frac{\|\boldsymbol{B}^{\mathrm{T}}\boldsymbol{C}^{\mathrm{T}}\boldsymbol{S}\|^2}{\varepsilon}\bar{\rho}^2 + P(\|\boldsymbol{B}^{\mathrm{T}}\boldsymbol{C}^{\mathrm{T}}\boldsymbol{S}\|)\rho$$
$$+ c_0\left[-\psi_0\bar{c}_0 + P(\|\boldsymbol{B}^{\mathrm{T}}\boldsymbol{C}^{\mathrm{T}}\boldsymbol{S}\|)\right]$$
$$+ c_1\left[-\psi_1\bar{c}_1 + P(\|\boldsymbol{B}^{\mathrm{T}}\boldsymbol{C}^{\mathrm{T}}\boldsymbol{S}\|)\|\boldsymbol{x}\|\right] + \ldots$$
$$+ c_N\left[-\psi_N\bar{c}_N + P(\|\boldsymbol{B}^{\mathrm{T}}\boldsymbol{C}^{\mathrm{T}}\boldsymbol{S}\|)\|\boldsymbol{x}\|^N\right]$$

$$= -\boldsymbol{S}^{\mathrm{T}}\boldsymbol{K}_{\mathrm{D}}\boldsymbol{S} - \frac{\|\boldsymbol{B}^{\mathrm{T}}\boldsymbol{C}^{\mathrm{T}}\boldsymbol{S}\|^2}{\varepsilon}\bar{\rho}^2$$
$$+ P(\|\boldsymbol{B}^{\mathrm{T}}\boldsymbol{C}^{\mathrm{T}}\boldsymbol{S}\|)\bar{\rho} - \psi_0 c_0\bar{c}_0 - \psi_1 c_1\bar{c}_1 - \ldots - \psi_N c_N\bar{c}_N \quad (B4)$$

The term $-\frac{\|\boldsymbol{B}^{\mathrm{T}}\boldsymbol{C}^{\mathrm{T}}\boldsymbol{S}\|^2}{\varepsilon}\bar{\rho}^2 + P(\|\boldsymbol{B}^{\mathrm{T}}\boldsymbol{C}^{\mathrm{T}}\boldsymbol{S}\|)\bar{\rho}$ in Eq. (B4) is a

quadratic function of $\bar{\rho}$, and when $\bar{\rho} = \frac{P(\|\boldsymbol{B}^{\mathrm{T}}\boldsymbol{C}^{\mathrm{T}}\boldsymbol{S}\|)\varepsilon}{2\|\boldsymbol{B}^{\mathrm{T}}\boldsymbol{C}^{\mathrm{T}}\boldsymbol{S}\|^2}$, the term

reaches the maximum value of $\frac{\varepsilon\kappa^2}{4}$, where $\kappa = \max\left(\frac{g(x)}{x}\right)$ is

defined in Condition 1. Thus we may write the inequality as

$$\dot{V} \leqslant -\boldsymbol{S}^{\mathrm{T}}\boldsymbol{K}_{\mathrm{D}}\boldsymbol{S} + \frac{\varepsilon\kappa^2}{4} - \psi_0 c_0\bar{c}_0 - \psi_1 c_1\bar{c}_1 - \ldots - \psi_N c_N\bar{c}_N$$

$$= -\boldsymbol{S}^{\mathrm{T}}\boldsymbol{K}_{\mathrm{D}}\boldsymbol{S} + \frac{\varepsilon\kappa^2}{4} - \psi_0\left(\frac{1}{2}c_0 - \bar{c}_0\right)^2 - \psi_1\left(\frac{1}{2}c_1 - \bar{c}_1\right)^2$$
$$- \ldots - \psi_N\left(\frac{1}{2}c_N - \bar{c}_N\right)^2 + \kappa_1$$

$$= -\boldsymbol{S}^{\mathrm{T}}\boldsymbol{K}_{\mathrm{D}}\boldsymbol{S} - \psi_0\left(\frac{1}{2}c_0 - \bar{c}_0\right)^2 - \psi_1\left(\frac{1}{2}c_1 - \bar{c}_1\right)^2 - \ldots$$
$$- \psi_N\left(\frac{1}{2}c_N - \bar{c}_N\right)^2 + \kappa_2 \quad (B5)$$

where $\kappa_2 = \kappa_1 + \frac{\varepsilon\kappa^2}{4}$ is a constant.

With Eqs. (B3) and (B5), we may conclude that the closed loop system is of uniformly ultimate boundedness using the results in Ref.[42].

## References

1. Ehrenwald L, Guelman M. Integrated adaptive control of space manipulators. *J Guid Control Dyn* 1998;**21**(1):156–63.
2. Guo YS, Chen L. Adaptive neural network control for coordinated motion of a dual-arm space robot system with uncertain parameters. *Appl Math Mech* 2008;**29**(9):1131–40.
3. Jia YH, Hu Q, Xu SJ. Dynamics and adaptive control of a dual-arm space robot with closed-loop constraints and uncertain inertial parameters. *Acta Mech Sinica* 2014;**30**(1):112–24.
4. Flores-Abad A, Wei Z, Ma O, Pham K. Optimal control of space robots for capturing a tumbling object with uncertainties. *J Guid Control Dyn* 2014;**37**(6):2014–7.
5. Green A, Sasiadek JZ. Intelligent tracking control of a free-flying flexible space robot manipulator. *AIAA guidance, navigation and control conference and exhibit*; 2007 Aug 20–23; Hilton Head, South Carolina. Reston: AIAA; 2007. p. 132–56.
6. Meirovitch L, Chen Y. Trajectory and control optimization for flexible space robots. *J Guid Control Dyn* 1995;**18**(3): 493–502.
7. Billing-Ross JA, Wilson JF. Pointing system design for low-disturbance performance. *AIAA guidance, navigation, and control conference*; 1988 Aug 15–17; Minneapolis (MN). Reston: AIAA; 1988. p. 444–51.
8. Osuka K, Yoshida K, Ono T. New design concept of space manipulator-a proposal of torque-unit manipulator. *Proceedings of the 33rd conference on decision and control*; 1994 Dec 14–16; Lake Buena Vista (FL). Piscataway (NJ): IEEE Press; 1994. p. 1058 1823–5.
9. Peck MA, Paluszek MA, Thomas SJ, Mueller JB. Control-moment gyroscopes for joint actuation: A new paradigm in space robotics. *Proceedings of the 1st space exploration conference: continuing the voyage of discovery*; 2005 Jan 30–Feb 1; Orlando (FL). Reston: AIAA; 2005. p. 204–33.
10. Peck MA. Low-power, high-agility space robotics. *AIAA guidance, navigation and control conference and exhibit*; 2005 Aug 15–18; San Francisco (CA). Reston: AIAA; 2005. p. 3759–70.
11. Carpenter MD, Peck MA. Dynamics of a high-agility, low-power coelostat telescope. *AIAA guidance, navigation and control conference and exhibit*; 2006 Aug 21–24; Keystone (CO). Reston: AIAA; 2006. p. 4175–91.
12. Carpenter MD, Peck MA. Minimum-power robotic maneuvering using control-moment gyroscopes. *AIAA guidance, navigation and control conference and exhibit*; 2007 Aug 20–23; Hilton Head (SC). Reston: AIAA; 2007. p. 210–22.
13. Carpenter MD. Power-optimal steering of a space robotic system driven by control-moment gyroscopes. *AIAA guidance, navigation and control conference and exhibit*; 2008 Aug 18–21; Honolulu (HI). Reston: AIAA; 2008.
14. Brown D, Peck MA. Scissored-pair control-moment gyros: a mechanical constraint saves power. *J Guid Control Dyn* 2008;**31** (6):1823–6.
15. Brown D. Control moment gyros as space-robotics actuators. *AIAA guidance, navigation and control conference and exhibit*; 2008 Aug 18–21; Honolulu (HI). Reston: AIAA; 2008.
16. Brown D, Peck MA. Energetics of control moment gyroscopes as joint actuators. *J Guid Control Dyn* 2009;**32**(6):1871–83.
17. Jia YH, Zhao N, Xu SJ. Trajectory tracking control of space robot actuated by control moment gyroscopes. *J Beijing Univ Aeronaut Astronaut* 2014;**40**(3):285–91 Chinese.
18. Zhao N, Jia YH, Xu SJ. Trajectory tracking control of a reactionless space robot. *Chin Space Sci Technol* 2014;**34** (2):13–21 Chinese.
19. Feng Y, Yu XH, Man ZH. Non-singular terminal sliding mode control of rigid manipulators. *Automatica* 2002;**38** (12):2159–67.
20. Ferrara A, Magnani L. Motion control of rigid robot manipulators via first and second order sliding modes. *J Intell Robot Syst Theory Appl* 2007;**48**(1):23–36.
21. Ferrara A, Incremona GP. Robust motion control of a robot manipulator via integral suboptimal second order sliding modes. *Proceedings of the 52nd IEEE conference on decision and control*; 2013 Dec 10–13; Florence, Italy. Piscataway (NJ): IEEE Press; 2013. p. 1107–12.
22. Yoo DS, Chung MJ. A variable structure control with simple adaptation laws for upper bounds on the norm of the uncertainties. *IEEE Trans Autom Control* 1992;**37**(6):159–65.
23. Leung TP, Zhou QJ, Su CY. An adaptive variable structure model following control design for robot manipulators. *IEEE Trans Autom Control* 1991;**36**(3):347–52.
24. Wheeler G, Su CY, Stepanenko Y. A sliding mode controller with improved adaptation laws for the upper bounds on the norm of uncertainties. *Automatica* 1998;**34**(12):1657–61.

25. Tao CW, Chan ML, Lee TT. Adaptive fuzzy sliding mode controller for linear systems with mismatched time-varying uncertainties. *IEEE Trans Syst Man Cybern B Cybern* 2003;**33**(2):283–94.

26. Muñoz D, Sbarbaro D. An adaptive sliding-mode controller for discrete nonlinear systems. *IEEE Trans Ind Electron*. 2000;**47**(3):574–81.

27. Plestan F, Shtessel Y, Brégeault V, Poznyak A. New methodologies for adaptive sliding mode control. *Int J Control* 2010;**83**(9):1907–19.

28. Cong BL, Liu XD, Chen Z. Improved adaptive sliding mode control for a class of second-order mechanical systems. *Asian J Control* 2013;**15**(6):1862–6.

29. Li P, Zheng ZQ. Robust adaptive second-order sliding-mode control with fast transient performance. *IET Control Theory Appl* 2012;**6**(2):305–12.

30. Wang L, Sheng YZ, Liu XD. A novel adaptive high-order sliding mode control based on integral sliding mode. *Int J Control* 2014;**12**(3):459–72.

31. Hughes PC. *Spacecraft attitude dynamics*. New York: John Wiley & Sons Inc.; 1986. p. 7–8.

32. Schaub H, Junkins JL. Stereographic orientation parameters for attitude dynamics: a generalization of the Rodrigues parameters. *J Astronaut Sci* 1996;**44**(1):1–19.

33. Jin YQ, Liu XD, Qiu W, Hou CZ. Time-varying sliding mode controls in rigid spacecraft attitude tracking. *Chin J Aeronaut* 2008;**21**(4):352–60.

34. Cong BL, Liu XD, Chen Z. Exponential time-varying sliding mode control for large angle attitude eigenaxis maneuver of rigid spacecraft. *Chin J Aeronaut* 2010;**23**(4):447–53.

35. Banerjee AK, Kane TR. Large motion dynamics of a spacecraft with a closed loop, articulated, flexible appendage. *Proceedings of the 25th AIAA structures, structural dynamics and materials conference*; 1984 May 14–16; Palm Springs (CA). Reston: AIAA; 1984.

36. Yoon H, Tsiotras P. Spacecraft adaptive attitude and power tracking with variable speed control moment gyroscopes. *J Guid Control Dyn* 2002;**25**(6):1081–90.

37. Schaub H, Vadali SR, Junkins JL. Feedback control law for variable speed control moment gyroscopes. *J Astronaut Sci* 1998;**46**(3):307–28.

38. Yoon H, Tsiotras P. Adaptive spacecraft attitude tracking control with actuator uncertainties. *AIAA guidance, navigation and control conference and exhibit*; 2005 Aug 15–18; San Francisco (CA). Reston: AIAA; 2005. p. 5311–22.

39. Senda K, Nagaoka H. Adaptive control of free-flying space robot with position/attitude control system. *J Guid Control Dyn* 1999;**22**(3):488–90.

40. De Wit CC, Olsson H, Åström KJ, Lischinsky P. A new model for control of systems with friction. *IEEE Trans Autom Control* 1995;**40**(3):419–25.

41. Walcott BL, Zak SH. Combined observer-controller synthesis for uncertain dynamical systems with applications. *IEEE Trans Syst Man Cybern* 1988;**18**(1):367–71.

42. Corless MJ, Leitmann G. Continuous state feedback guaranteeing uniform ultimate boundedness for uncertain dynamic systems. *IEEE Trans Autom Control* 1981;**26**(5):1139–44.

**Jia Yinghong** is an associate professor at School of Astronautics, Beihang University, Beijing, China. He received the Ph.D. degree from Harbin Institute of Technology in 2005. His current research interests are dynamics and control of space robot/multibody system, spacecraft attitude dynamics and control, and sliding mode control.

**Xu Shijie** is a professor and Ph.D. supervisor at School of Astronautics, Beihang University, Beijing, China. His current research interests are nonlinear orbital dynamics and control in deep space exploration, spacecraft dynamics and control, and robust control theory and application.